

Fall 12-18-2014

## Gas Detection Applications of Vertically Aligned Metal Oxide Nanowire Arrays

Haiqiao Su  
*University of New Orleans*, [hsu@uno.edu](mailto:hsu@uno.edu)

Follow this and additional works at: <https://scholarworks.uno.edu/td>



Part of the [Engineering Physics Commons](#)

---

### Recommended Citation

Su, Haiqiao, "Gas Detection Applications of Vertically Aligned Metal Oxide Nanowire Arrays" (2014).  
*University of New Orleans Theses and Dissertations*. 1947.  
<https://scholarworks.uno.edu/td/1947>

This Dissertation is protected by copyright and/or related rights. It has been brought to you by ScholarWorks@UNO with permission from the rights-holder(s). You are free to use this Dissertation in any way that is permitted by the copyright and related rights legislation that applies to your use. For other uses you need to obtain permission from the rights-holder(s) directly, unless additional rights are indicated by a Creative Commons license in the record and/or on the work itself.

This Dissertation has been accepted for inclusion in University of New Orleans Theses and Dissertations by an authorized administrator of ScholarWorks@UNO. For more information, please contact [scholarworks@uno.edu](mailto:scholarworks@uno.edu).

Gas Detection Applications of Vertically Aligned Metal Oxide Nanowire Arrays

A Dissertation

Submitted to the Graduate Faculty of the  
University of New Orleans  
in partial fulfillment of the  
requirements for the degree of

Doctor of Philosophy  
in  
Engineering and Applied Science  
Physics

By

Haiqiao Su  
M.S. University of Electronic Science and Technology of China, 2006  
B.S. University of Electronic Science and Technology of China, 2009

December, 2014

Copyright 2014, Haiqiao Su

To My Family

## Acknowledgments

The research in this dissertation for my Ph. D program was studied in Advanced Materials Research Institute (AMRI), University of New Orleans (UNO). Without the enormous help from my colleagues of AMRI, UNO and other institutes, this research would not be possible.

I would like to express my greatest gratitude to my advisor, Prof. Weilie Zhou, for his expertise in this field, for giving the opportunity to me to pursue my Ph. D, and his continuous support during this period. He is great patient and always gives me invaluable suggestions in my research as well as my life.

I would like to express my sincere appreciation for my academic committee members: Prof. Kevin Stokes, Prof. Leszek Malkinski, Prof. Ashok Puri, and Prof. Paul Schilling for their effort in reviewing and helpful suggestions on this dissertation.

Furthermore, I would like to thank Dr. Jiajun Chen, and Dr. Kai Wang for their helpful training in my first year and helpful suggestions on my research; I would like to thank my previous group members Dr. Chunming Liu, Dr. Zhijie Li, Dr. Baobao Cao, Dr. Zhongming Zeng, Dr. Kun Yao, and my present group members Satish Chandra Rai, Zhi Zheng, Sarah Wozny, Shuke Yan, Nooraldeen Alkurd for their valuable discussion in my research period.

I would like to dedicate this research work to my family and thank them all for their continuous support and guidance.

I would like to thank AMRI for continuous support of graduate assistantship during my Ph. D program. I gratefully acknowledge the financial supports from the DARPA Grant Nos.HR0011-07-1-0032, and Defense Threat Reduction Agency Contract through Surface Treatment Technologies Corporation.

# Contents

<b>Abstract</b> .....	<b>viii</b>
<b>Chapter 1 Introduction</b> .....	<b>1</b>
1.1 Gas Sensor .....	1
1.1.1 Gas Sensor Properties .....	2
1.1.2 Gas Sensors Based on Electrical Properties .....	4
1.1.2.1 Gas Sensors Based on Metal Oxide Semiconductor .....	5
1.1.2.2 Gas Sensors Based on Conducting Polymer .....	7
1.1.3 Gas sensors based on ionization .....	8
1.1.4 Gas Sensors Based on Piezoelectric Effect .....	9
1.1.5 Gas sensors based on surface acoustic waves .....	10
1.2 Electronic Noses .....	11
1.3 Metal Oxides .....	13
1.3.1 Metal Oxides for Gas Detection .....	13
1.3.2 Metal Oxides Synthesis Techniques .....	14
1.3.2.1 Physical Vapor Deposition (PVD) .....	14
1.3.2.1.1 Electron Beam Physical Vapor Deposition .....	15
1.3.2.1.2 Sputtering Deposition .....	16
1.3.2.2 Chemical Vapor Deposition (CVD) .....	17
1.3.2.3 Hydrothermal Synthesis .....	18
1.3.2.4 Sol-gel synthesis .....	19
1.3.2.5 Electrochemical deposition .....	20

1.4 Characterization Techniques for Gas Sensors.....	21
1.4.1 Sensor testing system.....	21
1.4.2 Targeting chemical concentration calculation.....	22
1.4.3 Sensor performance measurements.....	24
1.4.3.1 Gas sensors based on electrical properties.....	24
1.4.3.2 Gas sensors based on ionization.....	25
1.4.3.3 Gas sensors based on the piezoelectric effect.....	27
1.4.3.4 Gas sensors based on surface acoustic waves.....	28
1.5 Three Dimensional (3D) ZnO Nanowire Arrays for Gas Detection.....	30
<b>Chapter 2 Electronic noses based on core-shell metal oxides nanowire arrays.....</b>	<b>31</b>
2.1 Materials and methods.....	31
2.1.1 Wafer size random-distributed ZnO nanowire arrays.....	31
2.1.2 Patterned grown well-aligned ZnO nanowire arrays.....	32
2.2 Results and Discussion.....	34
2.2.1 Wafer size random-distributed ZnO nanowire arrays.....	34
2.2.2 Patterned grown well-aligned ZnO nanowire arrays.....	42
2.2.2.1 ZnO nanowire arrays with same lengths but different spacings.....	43
2.2.2.2 ZnO nanowire arrays with same spacings but different lengths.....	43
2.4 Conclusion.....	44
<b>Chapter 3 PEDOT:PSS/ZnO nanowire arrays VOC sensor.....</b>	<b>46</b>
3.1 Experiment.....	46

3.2 Results and discussions.....	48
3.3 Conclusions.....	51
<b>Chapter 4 Low voltage air ionization sensor with ZnO nano-rods electrode.....</b>	<b>52</b>
4.1 Experiment.....	53
4.2 Results and discussion.....	55
4.3 Conclusion.....	63
<b>Chapter 5 Self-powered active sensors based on 3D ZnO nanowire arrays.....</b>	<b>64</b>
5.1 Experiment.....	64
5.2 Result and discussion.....	66
5.3 Conclusions.....	70
<b>Chapter 6 ZnO nanowire arrays SAW sensor.....</b>	<b>71</b>
6.1 Experiment.....	71
6.2 Results and discussion.....	71
6.3 Conclusion and future plan.....	74
<b>Chapter 7 Conclusions.....</b>	<b>76</b>
<b>References.....</b>	<b>77</b>
<b>Vita.....</b>	<b>87</b>

## Abstract

To build novel electronic noses for mimicking biological olfactory systems that consist of olfactory receptor arrays with large surface area and massively-diversified chemical reactivity, three dimensional (3D) vertical aligned ZnO nanowire arrays were employed for gas detection, because ZnO nanowire arrays share 3D structures similar to mammalian olfactory receptor arrays, with thousands of vertical nanowires providing a high reception area which can significantly enhance the sensors' sensitivity. In this dissertation, several different types of gas sensors have been investigated based on 3D ZnO nanowire arrays, including gas sensors based on electrical properties, gas sensors based on the piezoelectric effect, gas sensors based on ionization, and gas sensors based on surface acoustic waves. For gas sensors based on electrical properties, ZnO nanowire arrays were decorated with different materials (such as SnO<sub>2</sub>, In<sub>2</sub>O<sub>3</sub>, WO<sub>3</sub> and PEDOT:PSS), and each array of nanowires can produce a distinguishable response for each separate analyte, which has provided a promising way to improve the selectivity of the gas sensor. Both patterned grown well-aligned and wafer size random-distributed 3D nanowire array sensing devices were studied. Gas sensors based on 3D metal oxides/ZnO vertical nanowire arrays have detected NO<sub>2</sub> and H<sub>2</sub>S down to ppb level, and five gases of NO<sub>2</sub>, H<sub>2</sub>S, H<sub>2</sub>, NH<sub>3</sub>, and CO have been discriminated. With the decoration by mixture of PEDOT:PSS polymer with metal oxide nanoparticles, ZnO vertical nanowire array gas sensors have fast response and recovery time as well as good sensitivity to volatile organic gases of acetone, methanol and ethanol. Active self-powered gas sensors based on 3D metal oxides/ZnO vertical nanowire arrays have been successfully fabricated. This gas sensor generates the power by itself and it showed different response to H<sub>2</sub>S and NO<sub>2</sub>

detection which could be employed to discriminate reducing and oxidizing gases. A novel ionization sensor has been built by ZnO vertical nanowire arrays, and with the decoration of metals, this device is able to ionize air under safe operation voltage under a magnetic field. Surface acoustic wave gas sensor has been fabricated based on ZnO nanowire arrays on piezoelectric ST-cut quartz substrates.

**Keywords:** Nanowires, Metal Oxides, 3D, Gas Sensors, sensitivity and selectivity.

## Chapter 1 Introduction

### 1.1 Gas Sensor

Gas sensor refers to the device which could detect environmental gases by interaction between its sensing part and gases. Two main parts of gas sensor are receptor and transducer. The output of the device would change after the receptor is exposed to certain gases compared with the initial output in air. The output change signal may also be transformed to real actions by the transducer, such as to sound alarms, or to turn on and off machines [1, 2].

Gas sensors have been applied and developed for long time since finding that exposure to certain gases can have a harmful effect on overall human health. Before the electrical gas sensor devices were invented, canaries, as the earliest gas sensors, were used to detect low oxygen or toxic atmospheres to protect miners in mining industry [3]. Safety lamps were also employed to detect low oxygen or flammable environments in mining industry [4]. Currently, more and more technologies have been explored for gas detection and have been applied in different areas depending on their specific advantages, such as low cost and easily fabricated metal oxide electrical gas sensors, high selectivity ionization gas sensors, and so on. Meanwhile, various sensing materials have been investigated to improve the gas detection performance. Right now, gas sensors are becoming more and more important to protect people lives and properties through detecting combustible, flammable and toxic gases, and they have been widely used and have great impact in the areas of environmental emission control, public security, automotive application, workplace hazard monitoring, medical diagnosis, and so on [5-7]. With the boom of nanotechnologies, nanomaterials have shown good sensing performance to various gases due to their large surface to volume ratio compared to bulk materials. My research focused on fabricating gas sensors based on 3D ZnO nanowire arrays and testing their performances. To take

advantage of extremely large surface areas of ZnO nanowire arrays, several types of gas sensors have been successfully fabricated and shown good sensing performances, including gas sensors based on electrical properties, gas sensors based on the piezoelectric effect, gas sensors based on ionization, and gas sensors based on surface acoustic waves.

### 1.1.1 Gas Sensor Properties

For gas sensors, researchers have always been pursuing high sensitivity and selectivity, as well as good stability and quick response and recovery time for real applications [8]. All these factors are used to judge the performance of the gas sensors.

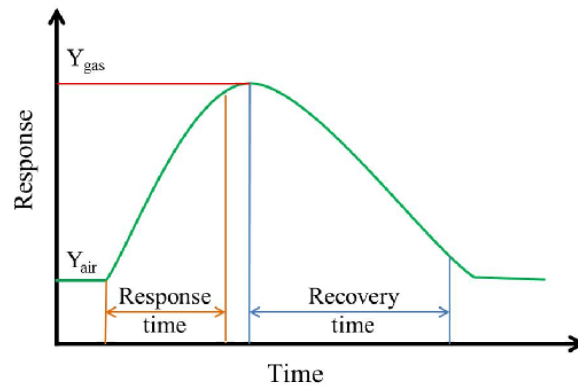


Figure 1.1 Typical response and recovery curve for n-type metal oxide semiconductor gas sensors in contact with reducing gases.

Sensitivity refers to the output change to initial output ratio of the gas sensor [9]. Output change is the difference between the output of the sensor in air and the sensor in a gas environment. If the sensor output “Y” is defined by the function  $Y=f(X)$ , then sensitivity “S” in targeting gas is:

$$S = \frac{Y_{gas} - Y_{air}}{Y_{air}} \times 100\% \quad (1.1)$$

Fig.1.1 is the typical response and recovery curve for n-type metal oxide semiconductor gas sensors in contact with reducing gases. From Fig.1.1, the sensitivity  $S$  could be calculated by  $Y_{\text{air}}$  and  $Y_{\text{gas}}$  which could be easily read on the curve. Bigger  $S$  values mean the device is more sensitive to certain gases and the gas could be easily detected at certain concentrations by the sensor device. Sensitivity is mostly related to the sensing materials as well as the mechanism of the sensing systems. On one hand, more materials are explored to reach high sensitivity. On the other hand, more techniques are studied based on current mature sensing materials. To compare the sensitivities from different materials or different techniques, all the sensor devices should be placed in the same targeting gas atmosphere. The sensitivity may also be affected by the operation temperatures. Elevated operation temperature may increase the sensitivity of some sensors, since the sensing materials become more active at higher temperature.

Another hot topic for gas sensor is to realize selective detection, which means to distinguish a targeting gas from interference gases [10]. Actually, most commercial sensors are applied to detect several different gases in real applications, for example, some are used to detect flammable gases, and some are used to detect toxic gases. However, these gas sensors could only tell the existence of flammable gases or toxic gases, but it is difficult to know what response gases are based on the testing results, since most sensors will respond to various gases. With the development of gas sensor techniques, lots of efforts are put to recognize what the gas is based on its response. The mostly popular way is to build gas sensor arrays in a sensing system. These sensors may have different sensing mechanisms as well as the same sensing mechanism. Data analysis techniques and gas response data bases are essential for sensor systems able to do selective detection.

Fast response and recovery time are crucial for gas sensors in real applications [11]. Fast response could better protect people lives and properties, and fast recovery time is the good for repeatable use of gas sensors. Response time is typically defined as the time duration from the

beginning to a certain percentage of a saturate response after the gas sensor is exposed to the targeting gas. For metal oxide semiconductor gas sensors, the response time is counted from beginning to 90% of saturate response, and recovery time is counted until the signal falls back to 10% of the saturated response, which is shown in Fig.1.1.

For real applications, the gas sensors should also be tested on their stabilities and detection limitations [7]. The stability refers to the time duration that the gas sensor could keep its sensitivity, selectivity, and response and recovery time. Detection limitation could be regarded as the resolution to specific gas of the gas sensor.

### 1.1.2 Gas Sensors Based on Electrical Properties

Gas sensors based on electrical properties are very common in our normal life and industry field. Usually, these sensors contain two or three electrodes connected by the sensing materials, as shown in Fig.1.2. The electrodes are typically fabricated by noble metals, and sensing materials are semiconducting or conducting materials. As two kinds of most popular sensing materials, metal oxide semiconductors and conducting polymers are highly investigated on this type gas sensor [12].

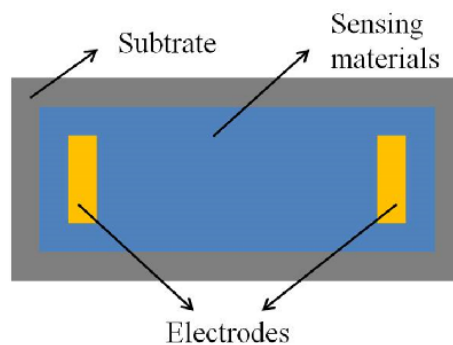


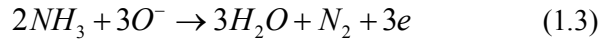
Figure 1.2 The electrical gas sensor.

### 1.1.2.1 Gas Sensors Based on Metal Oxide Semiconductor

Metal oxide semiconductor sensing materials have been widely used to fabricate gas sensor to detect trace amount of flammable and toxic gases, such as H<sub>2</sub> and H<sub>2</sub>S. As one of the most common sensing materials, they have several advantages compared with other materials, such as low cost, material variety, good stability, high sensitivity and quick response time. As we know, metal oxide semiconductors can be classified to n-type and p-type semiconductors. Both of them have some sensing materials which could be employed to detect different gases. For example, n-type SnO<sub>2</sub> could detect H<sub>2</sub>S to part per billion (ppb) level, while p-type CuO could detect H<sub>2</sub>S to part per million (ppm) level [13]. All of the following metal oxides have shown the gas sensing capabilities: ZnO, SnO<sub>2</sub>, Cr<sub>2</sub>O<sub>3</sub>, Mn<sub>2</sub>O<sub>3</sub>, Co<sub>3</sub>O<sub>4</sub>, NiO, CuO, SrO, In<sub>2</sub>O<sub>3</sub>, WO<sub>3</sub>, TiO<sub>2</sub>, V<sub>2</sub>O<sub>3</sub>, Fe<sub>2</sub>O<sub>3</sub>, GeO<sub>2</sub>, Nb<sub>2</sub>O<sub>5</sub>, MoO<sub>3</sub>, Ta<sub>2</sub>O<sub>5</sub>, La<sub>2</sub>O<sub>3</sub>, CeO<sub>2</sub>, Nd<sub>2</sub>O<sub>3</sub> [13].

Generally, metal oxides could be divided into transition and non-transition metal oxides. Transition metal oxides (SnO<sub>2</sub>, In<sub>2</sub>O<sub>3</sub>) contain several oxidation states, while non-transition oxides (Al<sub>2</sub>O<sub>3</sub>) have only one oxidation state. Therefore, only transition metal oxides are able to be used as sensing materials because of their sensing mechanism [14]. Even though the sensing mechanism for metal oxide semiconductor gas sensors is not clear, but it could be explained by redox reactions between the targeting gases and oxide surface [15]. When the metal oxides are in contact with targeting gases, oxygen species distributed on the surface of the materials would react with molecules of targeting gases leading to the conductance change which could be detected by current meters. For example, when the n-type semiconductor gas sensors are exposed to reducing gases (H<sub>2</sub>S, NH<sub>3</sub>, CO, and H<sub>2</sub>), oxygen species on the surface would react with reducing gases and release the electrons back to the n-type metal oxides, leading to an increased conductivity. As described by





Highly sensitive metal oxide semiconductor gas sensors are usually operated at high temperature, since elevated temperature would increase the probability of gas molecule adsorption which would reaction with oxygen species afterward leading to large conductivity change of gas sensor. To increase the sensitivity, a possible way is to mix different metal oxides, since there is a synergistic effect between the two components. The mixtures of SnO<sub>2</sub>-ZnO and In<sub>2</sub>O<sub>3</sub>-ZnO have been proved to have better sensitivity than single material [16]. Moreover, the sensitivity could be moderated by tuning the ratios of each material in the composite, and it may provide a good way for selective detection by expanding the material varieties. It also could enhance the sensitivity of metal oxide gas sensor by coating noble metal catalyst, since the catalytic noble metals are able to dissociate the oxygen molecules to enhance the density of adsorbed oxygen species, which increase the reaction probability between oxygen species and targeting gases.

Two factors, ozone and water molecules, have been reported to affect the performance of the metal oxide gas sensors by changing the conductance of metal oxides [17]. Take n-type metal oxide as an example, ozone would react with electrons on the surface which will lower its conductivity, while water molecules will donate electrons by forming hydroxyl (OH<sup>-</sup>) ions on the surface, leading to increase the conductivity. Meanwhile, the remaining hydrogen atoms would react with oxygen atoms on the surface to increase conductivity. All these reactions are accompanied with the increasing or decreasing of oxygen ion species on metal oxide surface, which will affect the reaction probability between oxygen species and targeting gases.

### 1.1.2.2 Gas Sensors Based on Conducting Polymer

Although metal oxide semiconductor gas sensors have been widely used in many fields and have shown great performances to inorganic gases, such as NO<sub>2</sub>, researchers have also put lots of efforts on studying conducting polymer sensors for detecting certain volatile organic chemicals (VOCs) with low reducing and oxidizing properties, such as alcohols [18]. It is very necessary to detect and monitor harmful VOCs, since VOCs are very easy to be contacted in our lives and they are easy to be volatilized and inhaled at room temperature. When the conducting polymer active layers are in contact with VOCs, gas absorption will occur to change their physical or chemical properties. The sensing mechanism of conducting polymers can be involved into redox reactions as well as physical adsorption and desorption to change their volume, weight, and chain conformation leading to conductance change [19].

Conducting polymers have lots of merits as sensing materials for gas detection [20-22]. Conducting polymer gas sensors are usually operated at room temperature due to the strong interaction between conducting polymer and gas analyte at room temperature, since the adsorption and desorption between conducting polymer and gas analyte are easily proceeded at room temperature. Furthermore, Conducting polymer gas sensors are much easier to be fabricated because most conducting polymers could be solved into liquid phase by introducing long side chains. The liquid phase is easily to be made into sensing films by casting or spin coating processes. Also conducting polymers are flexible and could be suitable for all kinds of sensor configurations without affecting their sensing properties. For VOCs detection, conducting polymer gas sensors possess high sensitivity and short response time. Also conducting polymers may be good candidates for selective detection because of their diversities. Polymer poly (3, 4 ethylenedioxythiophene) : poly (styrenesulfonate) (PEDOT:PSS) is one of the most stable conducting polymers and has been extensively studied because of its excellent film forming ability and high conductivity [23].

### 1.1.3 Gas sensors based on ionization

Ionization sensors are based on unique ionization characteristics of distinct gases. Fig.1.3 shows the basic configuration of ionization sensor consisting anode and cathode electrodes powered by DC voltage source [24]. The gas atom and molecule between the anode and cathode could be ionized by the strong electric field, and current flow generated by ionized electrons and ions could be measured. Since ionization sensors are working by unique ionization characteristics of distinct gases and each gas has a unique electrical breakdown voltage at constant temperature and pressure, they are good at selective gas detection and mainly used in advanced gas detection and monitoring for high precision measurement. However, the ionization sensors usually are huge and operated at risky high voltage, which hinders its applications [25].

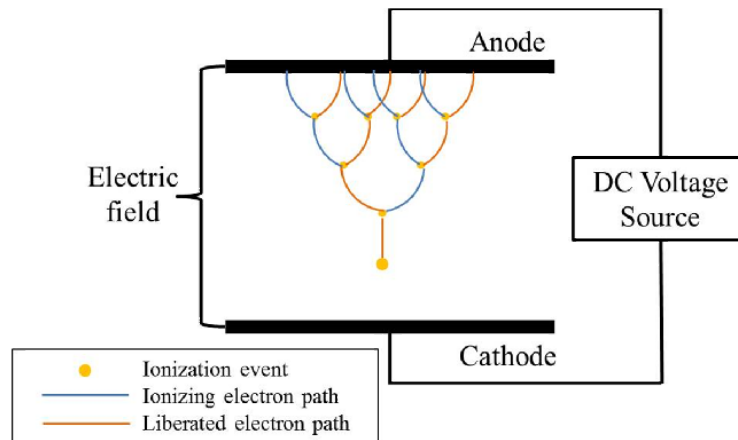


Figure 1.3 Avalanche effect between two electrodes under electric field.

During ionization process, positive ions and free electrons would be generated by strong electric field. Positive ions are produced when an atom or a molecule loses electrons by transferring sufficient energy which may come from electronic field or collisions with other atoms, molecules and ions. In the process, negative ions may be produced when an atom or a molecule traps free electrons by collision with them [26-28]. Fig.1.3 shows the process to create positive ions and free electrons by ionization between two electrodes under electric field, which

could be explained by avalanche effect [29]. At beginning, the gas atoms or molecules can be ionized by strong electric field, and the positive ions will drift towards the cathode electrode, while the free electrons will drift towards the anode electrode under the electric field. Assuming the free electron gained sufficient energy under the electric field, if it collides with another atom or molecule, one more electron can be liberated from the collided atom or molecule. Then, the two free electrons will travel towards the anode electrode, and more electrons can be liberated by collisions with more atoms and molecules if the free electrons still have sufficient energy. The chain reaction will keep going to generate more and more electrons and positive ions. The avalanche effect could be sustained until the electrons do not have enough energy for next collision. All the positive and negative ions generated under the electric field would contribute to the current flow detected by the current meter.

#### **1.1.4 Gas Sensors Based on Piezoelectric Effect**

Gas sensors based on piezoelectric effect is usually called self-powered gas sensor. The self-powered gas sensors have two functions [30]. One is to generate power by itself, and the other one is to detect interested gas atmosphere. To realize self-powered gas sensor device, the device must be made of piezoelectric materials possessing sensing properties. ZnO nanowire arrays have been highly reported as gas sensors and nano-generators. When ZnO crystal is under strain, the strained lattice will cause the change in band gap leading to piezoresistance effect, and the electrical conductance would change. ZnO nanowire has great sensitivity and selectivity compared with thin film or buck counterparts due to extremely high surface-to-volume ratio. P-type polymer coating could highly increase the output of the ZnO nanowire nanogenerator because p-type polymer captures n-type carriers on the surface and less n-type carriers could reduce the screening effect on the piezoelectric polarization charges [31]. Similarly, oxidizing or reducing gas will capture or release free electrons on ZnO nanowire. The free electrons change

would influence the screening effect on piezoelectric polarization charges to affect the piezoelectric output. Therefore, the signal change on piezoelectric out would reflect the influence of gas atmospheres. Therefore, ZnO nanowire is a good candidate for building self-powered gas sensors.

### **1.1.5 Gas sensors based on surface acoustic waves**

Surface acoustic wave (SAW) sensors have superior performance for gas detection due to high sensitivity, high stability, high accuracy and low cost [32]. SAW sensors involve in the transformation between electrical signal and mechanical wave. Most modern SAW sensors are using the inter-digitated transducer (IDT) for conversion between the electrical signal and the acoustic wave. The SAW sensor device is usually made on the piezoelectric substrate. The input IDT and output IDT are fabricated on two sides of substrate surface, and the sensing materials are deposited on the middle part of the substrate surface, as shown in Fig.1.4. The IDTs consist of two adjacent sets of finger electrodes [33].

The mechanical wave generated by piezoelectric substrate is first converted from the input sinusoidal electrical signal on input IDTs [34-36]. On the input IDTs, the input sinusoidal electrical signals cause the direction alternation of the electric field between two sets of finger electrodes, which leads to create alternating regions of tensile and compressive strain between finger electrodes by piezoelectric substrate, producing a mechanical wave at the substrate surface. And then, the mechanical wave would be converted back to sinusoidal electrical signal on output IDTs by piezoelectric substrate. Wavelength of the mechanical wave equals the spacing of two set finger electrodes on the same side. Since the mechanical wave is very sensitive to stimulus, the change between input and output signals could be detected to determine the stimulus. The stimulus could be physical such as a pressure, temperature, mass or strain change, and be chemical such as reaction with chemical gases [37]. Physical stimulus of pressure, temperature

and strain would change the length of substrate, leading to spacing change of IDTs. Additional mass could also be detected since it will decrease the mechanical wave velocity.

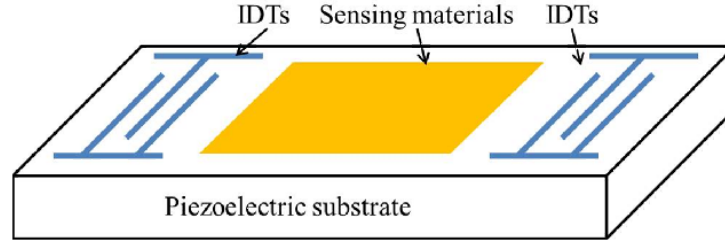


Figure 1.4 Schematic diagram of SAW device.

Generally, SAW devices have a high acoustic energy density on top surface of piezoelectric substrate. For thin film SAW devices, the central frequency changes, and the relationship between the change of central frequency or frequency shift ( $\Delta f$ ) versus the sheet conductivity ( $\sigma_s$ ) of the film can be described as:

$$\frac{\Delta f}{f_0} \propto \frac{\Delta v}{v_0} \approx -\frac{K^2}{2} \frac{\sigma_s^2}{\sigma_s^2 + v_0^2 C_s^2} \quad (1.6)$$

Where  $K_2$  is an electromechanical coefficient,  $v_0$  is the unperturbed SAW velocity,  $C_s = \epsilon_0 + \epsilon_p$ , is the sum of permittivity of the region above the film on the substrate,  $\sigma_s$  is the sheet conductivity of the sensing film [38]. The frequency shift will reflect the sensitivity of SAW sensor.

## 1.2 Electronic Noses

With booming of sensor technology and instruments, researchers are aiming to build a novel sensing system-electronic nose which is capable to mimic mammalian olfactory system using sensor arrays and pattern recognition systems, as shown in Fig.1.5. To mimic human olfaction system, electronic noses should perform with functions of identification, comparison, and quantification, including data storage and retrieval processes [39-41].

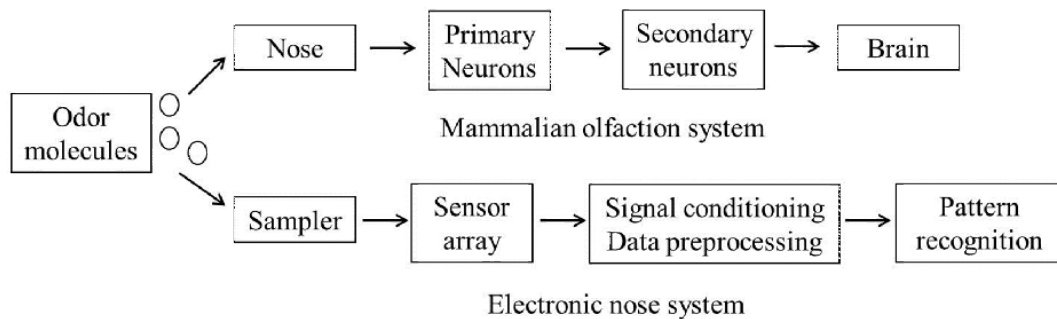


Figure 1.5 Block diagrams for mammalian olfaction system and electronic nose system.

Fig.1.5 shows the diagram of mammalian olfactory system. The odor molecules would first contact with olfactory receptors in olfactory epithelium after being inhaled into nose. The stimulus from odor molecules would be transduced into electrical signals which will be received by neuron system. The neuron system would recognize the odor in the memory, and the concentration of the odor may also be identified by the strength of the stimulus [42].

Similar with mammalian olfactory system, the electronic nose system consists of three main parts-sample delivery system, detection system and data analysis system to generate signal pattern for characterizing gas species. The sample delivery system enables to constantly deliver the targeting species into detection system. And the detection system is built by sensor arrays which could detect different targeting species. The sensing signals will be delivered to data analysis system once the sensor arrays contacts and reacts with the targeting species. All the output signals will be analyzed to compare with the database information to interpret the testing results [42].

Sensitivity and selectivity are two main factors for all gas sensors. And highly sensitivity and selectivity gas sensors would strongly support the electronic nose systems. Therefore, all the sensing techniques and systems mentioned above could be employed to construct the electronic nose systems. The diversities sensing techniques may provide different ways to realize electronic nose, since each techniques have their own advantages compared with each other [43].

## 1.3 Metal Oxides

### 1.3.1 Metal Oxides for Gas Detection

Metal oxide semiconductor gas sensors have been described a lot, which have various merits of low cost, simple fabrication, high sensitivity, long durability, good stability and so on [44]. However, besides working as semiconductor sensing materials, metal oxides also have been widely used in SAW sensors. For example, ZnO SAW sensors have been studied and reported by lots of researchers, not only because ZnO is easily to react with chemical species, but also ZnO is good piezoelectric materials [45]. With ZnO film coating, SAW sensors could be fabricated on non-piezoelectric or weakly piezoelectric substrates. To solve the ionization gas sensor drawbacks of high power consumption, huge structure and risky operation high-voltage, a novel ZnO nanowire ionization sensor has been reported [46].

Thin film metal-oxide semiconductor gas sensors have been studied for long time and been used in different areas. However, these sensors have some disadvantages [47]. The sensitivity becomes poor if the sensor works at low gas pressure. If the sensor works at high temperature, the performance becomes unstable after long time heating. The problem is suggested to be ascribed to the limited surface-to-volume ratio for thin films. With the development of nanotechnology, metal oxide nanostructures have been paid much more interest for applications in highly sensitive and selective gas sensors due to their high aspect ratio, large surface area, and availability of versatile structures compared to their thin film counterparts [48]. Most of the metal oxides have been grown as nanostructures, such as nanoparticles [49], nanowires [50], nanobelts [51], and nanodendritic structure [52](shown in Fig.1.6), which have used as gas sensing materials patterned into gas sensor devices. The gas sensors based on metal oxide nano-materials have shown highly enhanced sensitivity over their thin film or bulk counterparts. For example, gas

sensors formed with  $\text{In}_2\text{O}_3$  nanoparticles, single nanowire or nanowire networks, can detect  $\text{H}_2\text{S}$  down to the ppb level at room-temperature [53].

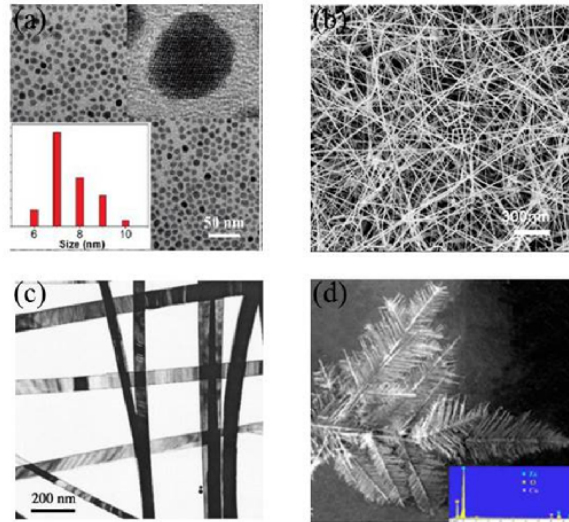


Figure 1.6 FESEM images of Nanomaterials (a)  $\text{In}_2\text{O}_3$  nanoparticles, (b)  $\text{In}_2\text{O}_3$  nanowires, (c)  $\text{SnO}_2$  nanobelts, and (d)  $\text{ZnO}$  nanodendritic structure.

### 1.3.2 Metal Oxides Synthesis Techniques

Various physical and chemical methods have been investigated for the synthesis of metal oxides materials in the forms of solid powder, thin film and nanowire. Each method has its own advantages and drawbacks. People may be interested in different methods for their particular applications. Several common methods are interpreted in below.

#### 1.3.2.1 Physical Vapor Deposition (PVD)

Physical vapor deposition (PVD) is a method to deposit thin films by the condensed vaporized material onto various substrate surfaces in vacuum system [54]. PVD involves pure physical processes, such as electron beam physical vapor deposition or plasma sputtering deposition. PVD could be used in industrial product manufacture, like semiconductor devices. Also, for scientific

purposes, PVD method has been developed to coat extreme thin films on small substrates [55].

The PVD system in our lab is PVD75 from Kurt J. Lesker Company, which is shown in Fig.1.7.

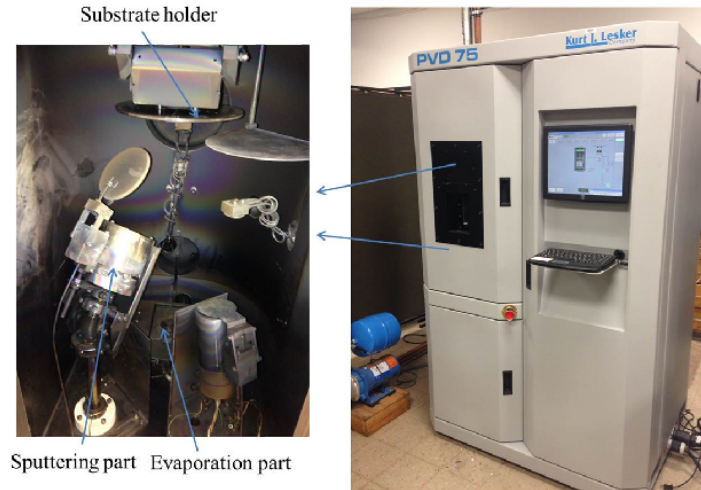


Figure 1.7 Image of PVD75 system.

### 1.3.2.1.1 Electron Beam Physical Vapor Deposition

Electron beam physical vapor deposition works in very high vacuum usually over than  $10^{-6}$  torr. The raw materials will be electron bombarded to high vapor pressure and then deposit to desired substrates [56].

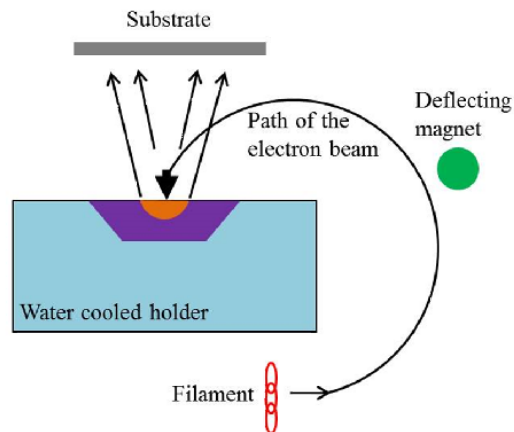


Figure 1.8 Diagram for electron beam physical vapor deposition.

Fig.1.8 is diagram for electron beam physical vapor deposition. In PVD75 system, the electron beam is generated by charged tungsten filament. The electron beam would be controlled by the magnetic field to precisely hit the raw materials in the sample holder. The substrate could be heated and rotated during deposition process in PVD75 system. For electron beam physical vapor deposition, the parameters should be taken care includes electron beam energy, distance between source and substrate, substrate temperature and orientation, and vacuum value [57].

### 1.3.2.1.2 Sputtering Deposition

The sputtering deposition is very commonly used for thin film deposition. During sputtering process, raw target material will be bombarded by energetic particles. When the particles' kinetic energy is much larger than conventional thermal energies, atoms will be ejected from sputtering target. In PVD system, the magnet under the source target will generate glow discharged plasma which will bombard the target materials and sputter some material away as a vapor [56].

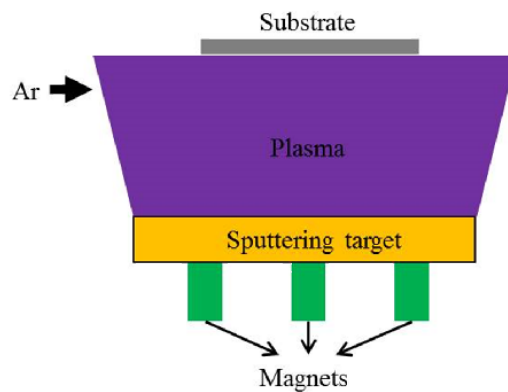


Figure 1.9 Diagram for sputtering deposition.

Fig.1.9 is diagram for sputtering deposition process. Ar is usually introduced into the chamber during sputtering process. Sputtering deposition could be influenced by distance between source and substrate, substrate temperature and orientation, and vacuum value. For deposit metal oxide,

low pressure oxygen is usually introduced to the system. Oxygen will be ionized with collision of electrons and vaporized source materials leading to better crystallinity and stoichiometry of the final products [58]. The deposition rate is usually controlled around  $5 \text{ \AA}/\text{sec}$  depending on the key parameters.

### 1.3.2.2 Chemical Vapor Deposition (CVD)

CVD method involves in chemical reaction between volatile precursors or between precursor and evaporated source materials to produce high purity desired product on certain substrate at elevated temperature in high vacuum system [59]. Several parameters should be fine adjusted to obtain the desired product, such as chamber pressure, vapor and substrate temperature, substrate materials and carrier gas. Fig.1.10 is the schematic diagram of a CVD system.

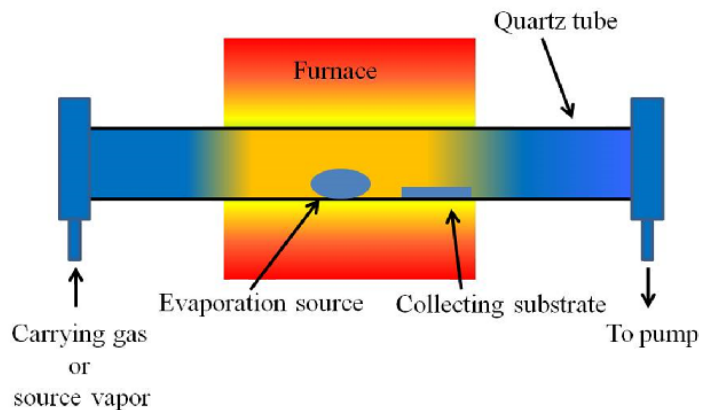


Figure 1.10 Schematic diagram of a CVD system.

CVD has been widely used to produce thin film and bulk materials in various forms, such as monocrystalline, polycrystalline, amorphous materials. Also CVD has been employed to grow nanomaterials, such as ZnO nanoparticles, ZnO nanowires, SnO<sub>2</sub> nanowires. One-dimensional structure growth could be explained by vapor liquid solid (VLS) growth mechanism [60]. Fig.1.11 is the schematics of nanowire growth by VLS process. For VLS growth, the noble metal

will be deposited on the substrate as catalyst. At certain elevated temperature, the noble metal catalyst will be melt to liquid which will adsorb the evaporated source materials. Once the adsorption becomes supersaturated, the nanowire will grow out and the growth is perpendicular to the solid-liquid interface. Longer nanowires would be obtained by introducing more source material and longer reaction time. Therefore, the size and position of nanowires would be determined by noble metal catalysts. In some situation, nanowires could be grown without noble metal catalyst, and the growth process could be considered as self-catalytic growth. For example, ZnO nanowires could be grown on Si substrate without catalyst [61].

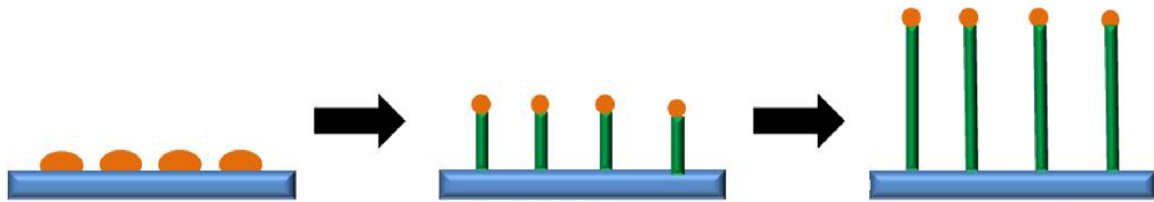
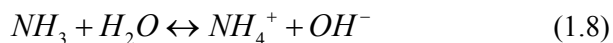
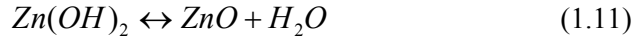
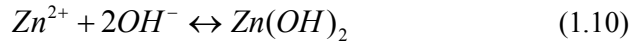


Figure 1.11 schematics for nanowire growth by VLS process.

### 1.3.2.3 Hydrothermal Synthesis

Hydrothermal synthesis is an aqueous solution based wet chemistry method. The precursor materials are first dissolved and the solution would be contained in autoclave (steel pressure vessel) where the chemical reaction occurs at certain elevated temperature [62]. For example, ZnO nanowire could be grown by hydrothermal method [63]. The precursor materials of  $Zn(NO_3)_2$  and hexamethylenetetramine (HMTA) ( $C_6H_{12}N_4$ ) are dissolved in distilled water [66]. The reaction in the solution may include:





The reaction is reversible for each step depending on the growth condition, such as precursor concentration, growth temperature and PH value of the solution. HMTA acting as a weak base and pH buffer may also facilitate ZnO anisotropic growth in [0001] direction by attaching to the nonpolar side facets of ZnO, since HMTA may act as as a bidentate Lewis base to coordinate and bridges two  $Zn^{2+}$  ions. HMTA is easy to hydrolyze in water and gradually produces HCHO and  $NH_3$ . The hydrolysis rate decreases with increasing pH and vice versa.  $NH_3$  would produce a base environment to form  $Zn(OH)_2$  and it is helpful to coordinate with  $Zn^{2+}$  and thus stabilizes the aqueous  $Zn^{2+}$ .  $Zn(OH)_2$  dehydrates into ZnO by heating. Generally, precursor concentration determines the ZnO nanowire density. Growth time and temperature control the ZnO nanowire morphology and aspect ratio.

#### 1.3.2.4 Sol-gel synthesis

The sol-gel synthesis is another solution based wet chemical method capable to synthesize metal oxide materials [64]. During sol-gel process, the liquid “sol” will be transited into solid “gel” by hydrolysis and condensation process. Usually, sol is stable colloidal suspension of tiny particles in solvent, and gel is a solid, jelly-like material, which is formed by agglomeration of particles. Sol-gel synthesis could fine control product chemical composition, since all the materials in the sol could be uniformly dispersed [65]. The sol-gel process may include mixing precursors, coating or casting sol into mold, gelation, aging the gel, drying, dehydration or chemical stabilization and densification. Processes of aging the gel, drying, dehydration or

chemical stabilization and densification may involve in heat treatment at different temperatures. Various forms of metal oxides could be made by sol-gel methods for different purposes, such as porous structures, thin films and dense powders.

### 1.3.2.5 Electrochemical deposition

Electrochemical deposition is able to deposit layer of metal and metal oxide on the conducting electrode. During electrochemical deposition process, cathode will collect hydrated ions under applied voltage [66]. Fig.1.12 is the schematic diagram of electrochemical deposition system. The materials used in this process must be electrochemically conductive, since electrical current must go through the deposit layer during the process. Both thin films and nanowires could be deposited by electrochemical deposition. Porous alumina oxide template is usually used to yield a dense array of parallel conductive nanowires.

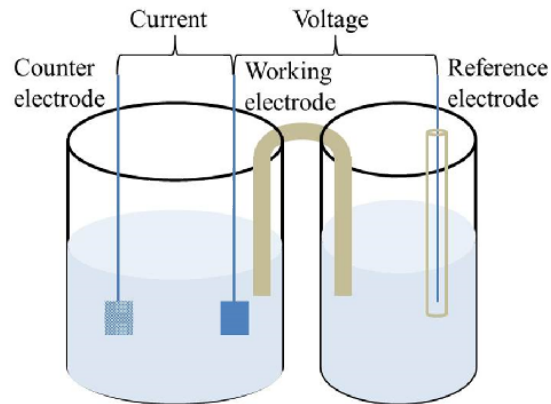


Figure 1.12 Schematic diagram of electrochemical deposition system.

The deposition process would be influenced by cathode potential, current density, deposition temperature, electrolyte composition and concentration, and all these parameters will control the product composition and morphology [67]. The big advantage of electrochemical deposition is

that it could control the growth structures with uniform length. The electrochemical depositions can be used to deposit both pure and doped metal oxide materials.

## 1.4 Characterization Techniques for Gas Sensors

### 1.4.1 Sensor testing system

The sensor testing system consists of a testing platform, a Keithley 2400 source unit, a Keithley 7001 switch module, and a computer collecting data, which is shown in Fig.1.13. The 2400 source unit supplies constant power source and detects the device electrical signals. The 7001 switch module has 40 channels to connect devices and switch testing among different devices. Computer program is used to control Keithley 2400 source unit and Keithley 7001 switch module.

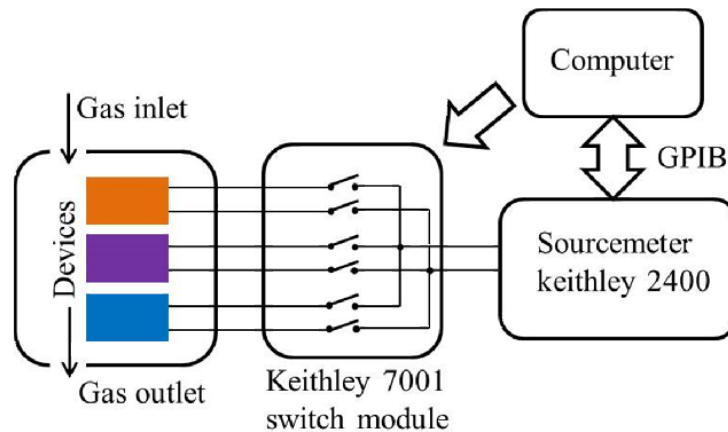


Figure 1.13 Schematic of the multi-sensor testing system.

The homemade gas sensor testing platform is shown in Fig.1.14. The testing system consists of sensor chamber, gas inlet and outlet fixed on the electrical testing board which has 28 connections. The volume of the chamber is around 50ml. The targeting gases would be injected into chamber from inlet by syringe. The outlet is connected to motor pump for purging the devices. Before testing, the sensor device would be loaded into the chamber and sealed by a glass on the top. The devices were connected to the electrical testing board by 0.02 mm gold wires and

silver paste. The glass should be covered by aluminum foil to block light during testing. The electrical signals for all the devices were continuously monitored when different air-diluted chemicals were introduced.

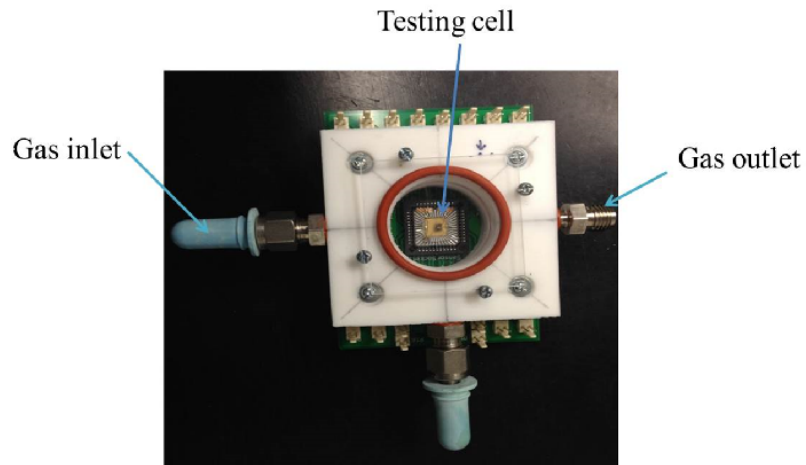


Figure 1.14 Photo image of homemade gas sensor testing platform.

#### 1.4.2 Targeting chemical concentration calculation

The chemicals tested in this dissertation include industrial gases of  $\text{H}_2\text{S}$ ,  $\text{NO}_2$ ,  $\text{H}_2$ ,  $\text{CO}$ ,  $\text{NH}_3$  as well as volatile organic gases of Acetone, Ethanol and Methanol. The sealed plastic bags of 1L volume are employed to dilute the five kinds of industrial gases, while three kinds of volatile organic gases are diluted using sealed bottles with 240 mL, which is shown in Fig.1.15.

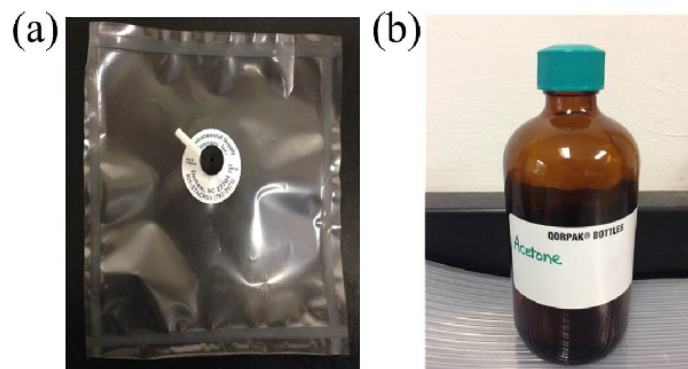


Figure 1.15 Photo image of (a) 1L plastic bag (b) 240 mL bottle.

The initial concentrations for all five purchased industrial gases are 2% diluted by N<sub>2</sub>. Table 1.1 shows the process to dilute 2% H<sub>2</sub>S to desired concentrations. Same method could be employed to dilute the other four industrial gases.

Table 1.1 Calculations for H<sub>2</sub>S gas testing concentrations (Chamber size: 50mL)

Initial concentration	Process	Pre-diluted concentration	Process	Final concentration in chamber
2%			Inject 2.5 mL of 2% H <sub>2</sub> S into chamber	1000ppm
	Inject 10 mL of 2% H <sub>2</sub> S into 1L gas bag	200ppm	Inject 0.5 mL of 200ppm H <sub>2</sub> S into chamber	2ppm
			Inject 0.25 mL of 200ppm H <sub>2</sub> S into chamber	1ppm
	Inject 10 mL of 200ppm H <sub>2</sub> S into 1L gas bag	2ppm	Inject 12.5 mL of 2ppm H <sub>2</sub> S into chamber	500ppb
			Inject 5 mL of 2ppm H <sub>2</sub> S into chamber	200ppb
			Inject 2.5 mL of 2ppm H <sub>2</sub> S into chamber	100ppb
			Inject 1.25 mL of 2ppm H <sub>2</sub> S into chamber	50ppb
			Inject 0.5 mL of 2ppm H <sub>2</sub> S into chamber	20ppb

The initial concentrations for three volatile organic gases are calculated by their saturated vapor pressures at room temperature. The saturated vapor pressures for Acetone, Ethanol and Methanol are around 200mmHg, 50mmHg, and 100mmHg at room temperature. Compared with standard atmosphere pressure of 760mmHg, their concentrations of saturated vapors are around 26%, 6.5%, and 13% at room temperature. The saturated vapor would be injected into 240mL bottles to dilute to desired concentration, which process is similar with the process to dilute 2% H<sub>2</sub>S.

### 1.4.3 Sensor performance measurements

#### 1.4.3.1 Gas sensors based on electrical properties

For measurement of gas sensors based on electrical properties, the current through gas sensor device is continuously tested under constant voltage. The schematic of 3D nanowire array gas sensor devices based on electrical properties is shown in Fig.1.16. In Fig.1.16a, 3D nanowire array is coated by metal oxides. The device is loaded into homemade platform and both top and bottom gold electrodes are deposited which will be connected to electrical testing board on homemade platform. In Fig.1.16b, two side bottom gold electrodes are fabricated on 3D nanowire array coated by polymers due to the limitation of process to fabricate top electrodes. The process to fabricate top electrode is described in chapter 2. Fig.1.16c is the photo image of real device.

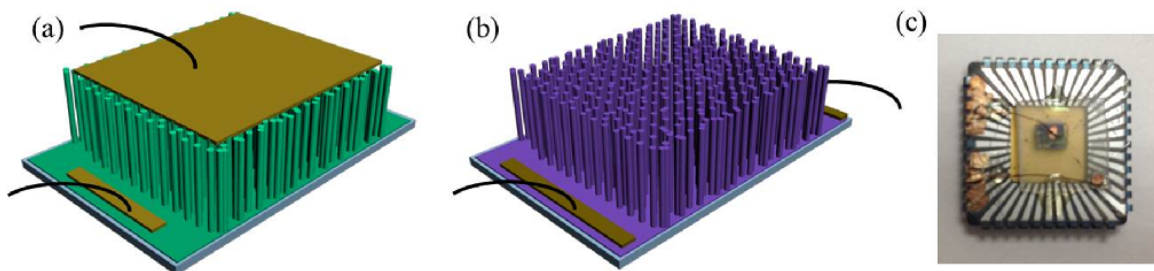


Figure 1.16 Schematics of 3D nanowire array gas sensor devices based on electrical properties (a) metal oxide coating (b) polymer coating (c) real device on sample hold.

Fig.1.17 is the typical current-time curve of 3D nanowire array gas sensor devices based on electrical properties in targeting gas under constant voltage. The sensitivity of the device to targeting gas under certain concentration is:

$$S = \frac{C_{gas} - C_{air}}{C_{air}} \times 100\% \quad (1.12)$$

The response time could be counted (duration from gas injection to 90% of saturated sensing response).

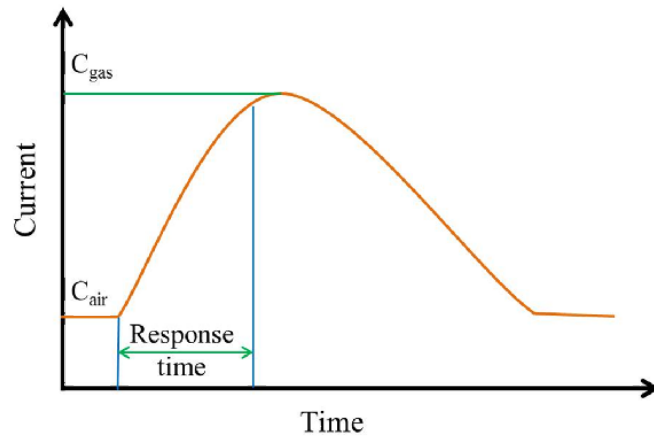


Figure 1.17 Typical current-time curve of 3D nanowire array gas sensor devices based on electrical properties in targeting gas under constant voltage.

### 1.4.3.2 Gas sensors based on ionization

For measurement of gas sensors based on ionization, current-voltage curve is continuously tested. Fig.1.18a is schematics of 3D nanowire array gas sensor device based on ionization. Fig.1.18b shows the anode and cathode of real 3D ZnO nanowire ionization gas sensor before packaging. The insulator spacer (surlyn) with 200 $\mu$ m thickness was cut off a square in the middle to cover the four sides of the anode substrate and ensure ZnO nanowire arrays is exposed. The

gold cathode substrate was carefully put on the spacer and the gold film is facing to the anode substrate. The spacer is sandwiched by the anode and cathode substrate. Then, all of them were placed on the hot plate for 30 seconds at 150°C. The spacer would stick the anode and cathode together.

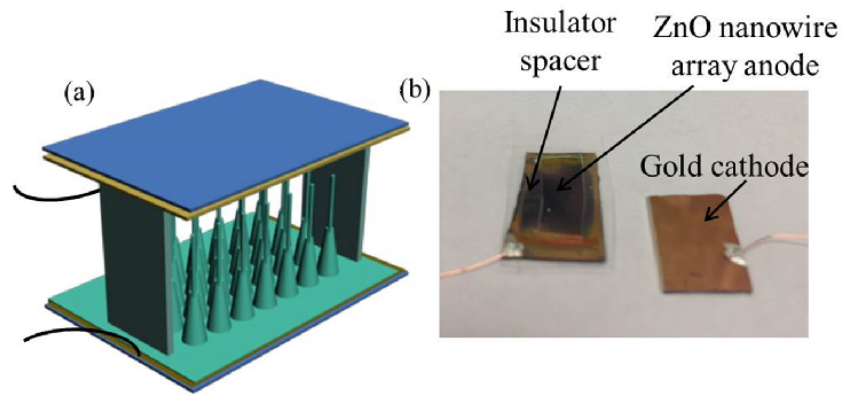


Figure 1.18 Schematics of 3D nanowire array gas sensor device based on ionization.

The device is loaded into homemade platform and both anode and cathode electrodes are connected to electrical testing board on homemade platform. In this dissertation, the ionization gas sensor has also been tested under magnetic field, which is shown in Fig.1.19. The magnetic field is generated by permanent magnets and the intensity is measured by Lakeshore 450 Gaussmeter.

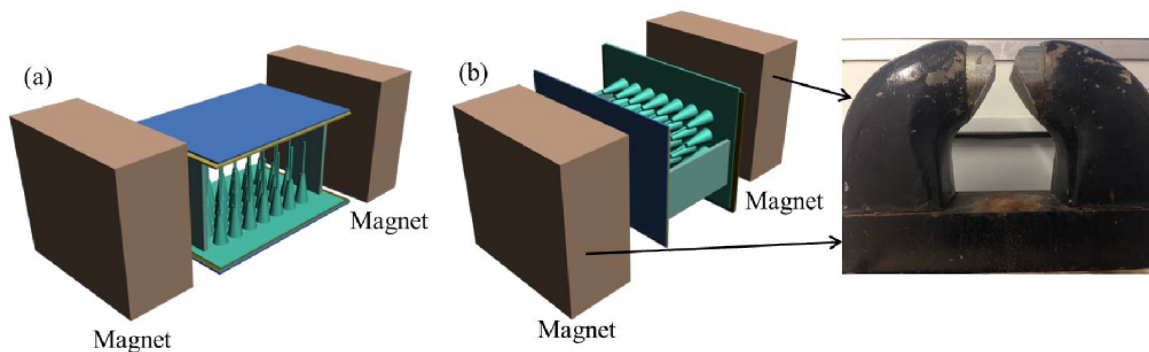


Figure 1.19 Schematics of 3D nanowire array gas sensor device based on ionization under magnetic field (a) transverse magnetic field and (b) longitudinal magnetic field.

Fig.1.20 is the typical current-voltage curve of 3D nanowire array gas sensor devices based on ionization in targeting gas. The sensitivities of the devices to targeting gas under certain concentration will be compared by the breakdown voltage.

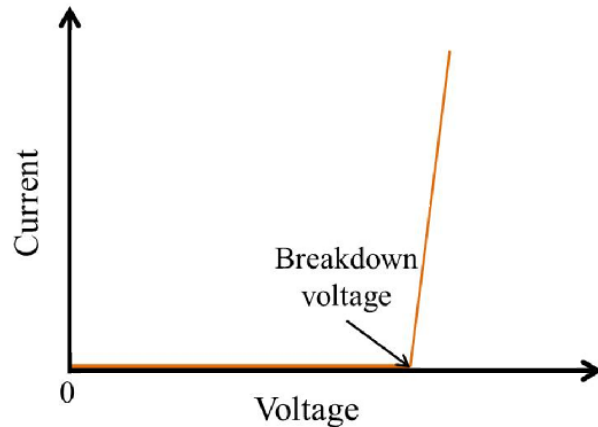


Figure 1.20 Typical current-voltage curve of 3D nanowire array gas sensor devices based on ionization in targeting gas.

### 1.4.3.3 Gas sensors based on the piezoelectric effect

For measurement of gas sensors based on piezoelectric effect, voltage-time curve is continuously tested under constant power without input power. Fig.1.21 is schematics of 3D nanowire array gas sensor devices based on piezoelectric effect. Top and bottom electrodes are connected to electrical testing board on homemade platform. In this measurement, the sealing glass on the top of the platform is replaced by flexible plastic film, since glass is rigid and it could not transfer the force to the device.

Fig.1.22 is the typical voltage-time curve of 3D nanowire array gas sensor devices based on piezoelectric effect in targeting gas under constant force. The sensitivity of the device to targeting gas under certain concentration is:

$$S = \frac{V_{gas} - V_{air}}{V_{air}} \times 100\% \quad (1.13)$$

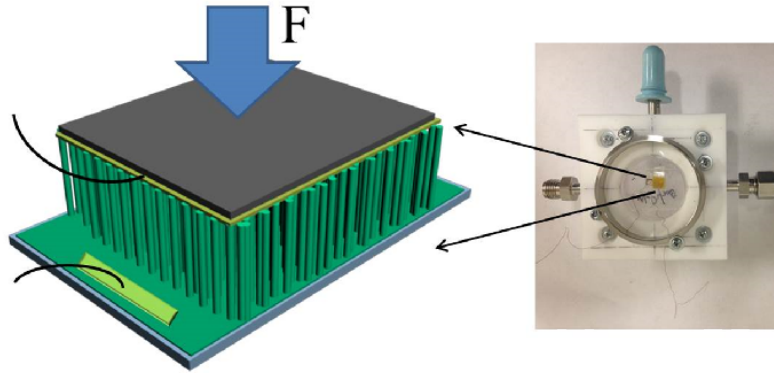


Figure 1.21 Schematics of 3D nanowire array gas sensor device based on piezoelectric effect.

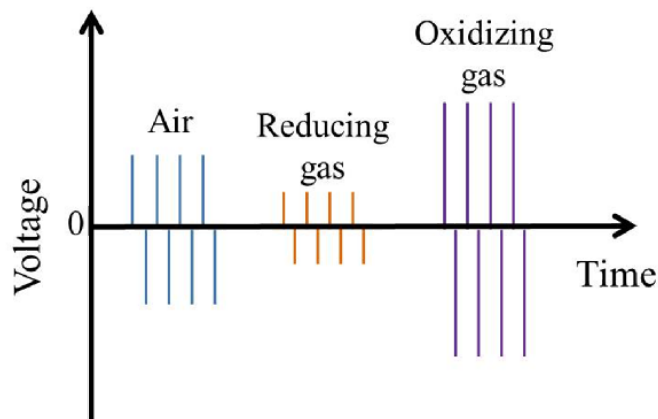


Figure 1.22 Typical voltage-time curve of 3D nanowire array gas sensor devices based on piezoelectric effect in targeting gas under constant force.

#### 1.4.3.4 Gas sensors based on surface acoustic waves

For measurement of gas sensors based on surface acoustic waves, frequency-time curve is continuously tested. Fig.1.23 is schematics of 3D nanowire array gas sensor devices based on

surface acoustic waves. The device is loaded into homemade platform and both input and output IDTs are connected to electrical testing board.

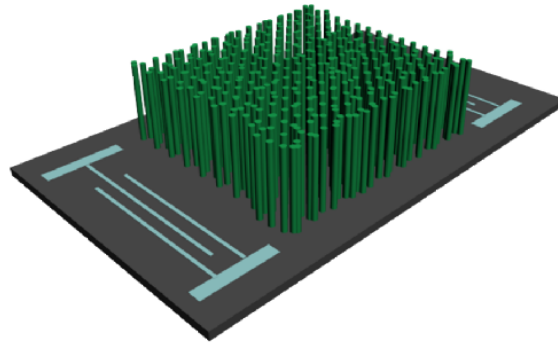


Figure 1.23 Schematics of 3D nanowire array gas sensor device based on surface acoustic wave.

Fig.1.24 is the typical frequency-time curve of 3D nanowire array gas sensor devices based on surface acoustic waves in targeting gas. The sensitivity of the device to targeting gas under certain concentration will be reflected by frequency shift.

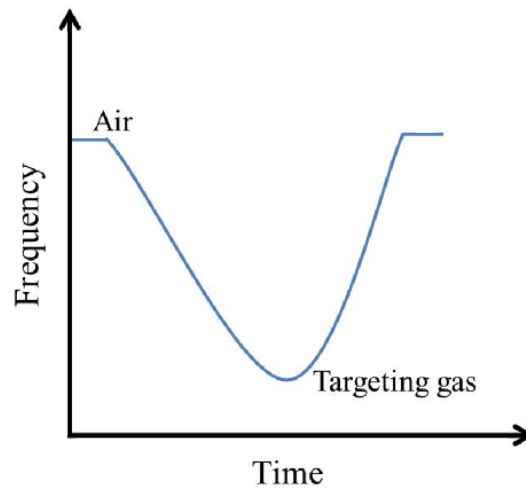


Figure 1.24 Typical frequency-time curve of 3D nanowire array gas sensor devices based on surface acoustic waves in targeting gas.

## 1.5 Three Dimensional (3D) ZnO Nanowire Arrays for Gas Detection

Metal oxide nanowire arrays share 3D structures similar to mammalian olfactory receptor arrays, with thousands of vertical nanowires providing a high reception area which can significantly enhance the sensors' sensitivity [68]. 3D ZnO nanowire arrays could be grown on various substrates by hydrothermal method and CVD method, and the morphology could be well controlled with assistance of e-beam lithography technique [69]. 3D ZnO nanowire arrays are rigid to be adapted to different kinds of sensor systems. 3D ZnO nanowire array could be employed to fabricate traditional semiconductor gas sensor which shows much better sensing performance than its thin film and bulk counterparts. Even more, with vertical aligned structure, 3D ZnO nanowire arrays could be easily functionalized by other sensing materials [8]. With different material decorations, each nanowire array can produce a distinguishable response for each separate analyte, which would provide a promising way to improve the selectivity. 3D ZnO nanowire arrays could be used to fabricate self-powered active gas sensor, since ZnO is not only a gas sensing material, but also a piezoelectric material which could generate power by outer strain. The output power generated by ZnO nanowire arrays is associated with the atmosphere. Reducing gases suppress output power of ZnO nanowire arrays, while oxidizing gas would enhance their output power [30]. ZnO nanowire arrays could be used to fabricate ionization gas sensor [29]. Especially, ionization gas sensors fabricated by ZnO nanowire arrays with sharp tips are capable to ionize targeting gases at much lower operation voltage compared with traditional ionization sensors, since sharp tip would highly enhance the intensity of electric field around it. ZnO nanowire arrays could also be good for SAW sensor due to extremely large surface [70].

## **Chapter 2 Electronic noses based on core-shell metal oxides nanowire arrays**

Electronic noses which are designed to detect and discriminate vapors using an array of sensors have been reported in many literatures, and most of them are fabricated by polycrystalline metal oxide thin film due to their various advantages mentioned above. In our experiment, a novel 3D electronic nose has been realized. For the purpose of mimicking the biological olfactory system with a diversity of receptor arrays, vertical 3D nanowire arrays have great potential, due to their extremely large surface area which provides a much stronger capability of capturing target molecules in the atmosphere. To realize multiple receptor arrays, different metal oxides were coated onto vertical ZnO nanowire arrays, which can be readily grown by hydrothermal synthesis. The electrical and gas-sensing properties of individual nanowire array were characterized. The electronic nose was fabricated with ZnO nanowire arrays decorated with different metal oxides and the gas discrimination of this electronic nose was studied in detail.

### **2.1 Materials and methods**

In this experiment, two different kinds of sensor modes were investigated. First one is created on wafer size random-distributed ZnO nanowire arrays, while second one is based on patterned grown well-aligned ZnO nanowire arrays.

To start the experiment,  $1 \times 1 \text{ cm}^2$  GaN/Al<sub>2</sub>O<sub>3</sub> (0001) substrates were prepared. These substrates were first cleaned by standard method (ultrasonically cleaned by acetone, isopropyl alcohol (IPA), and deionized water successively), and dried under a nitrogen flow, followed by growing vertical ZnO nanowire arrays in autoclave.

#### **2.1.1 Wafer size random-distributed ZnO nanowire arrays**

Fig. 2.1 shows the schematic of the fabrication procedures for wafer size random-distributed 3D sensor devices. Hydrothermal synthesis was employed for vertical ZnO nanowires growth on

1 x 1cm<sup>2</sup> GaN/Al<sub>2</sub>O<sub>3</sub> (0001) substrate [62]. The one step growth was carried out in the nutrition solution of 50 mM/L mixture of Zn(NO<sub>3</sub>)<sub>2</sub> and hexamethylenetetramine (HMTA) (C<sub>6</sub>H<sub>12</sub>N<sub>4</sub>) with 1:1 mass ratio in deionzied water at 80°C for 5 hours.

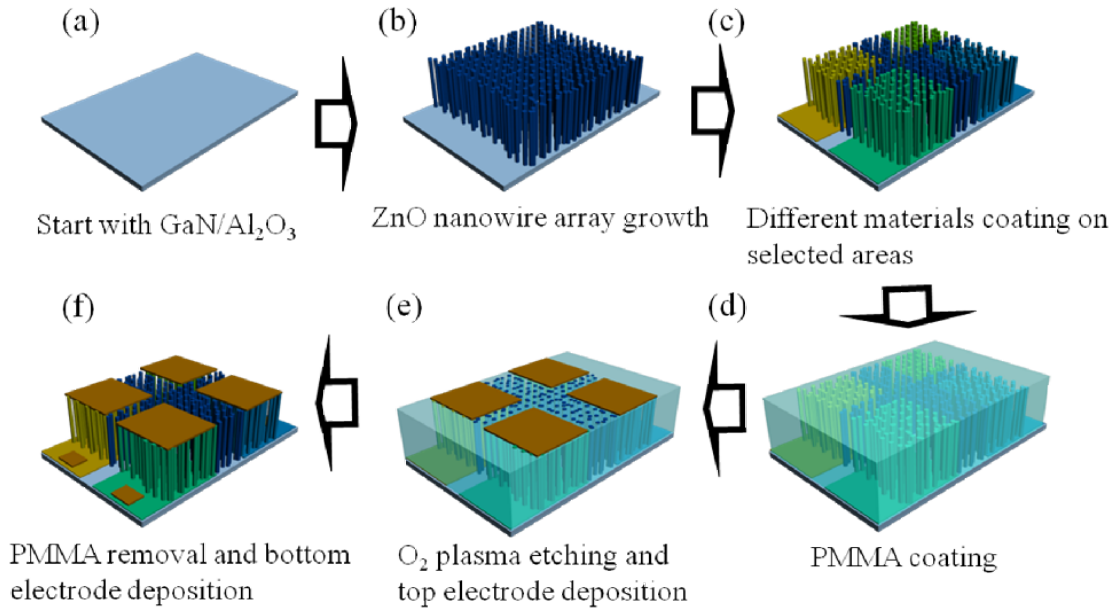


Figure 2.1 Schematic diagrams showing the procedures of 3-D gas sensor fabrication on wafer size random-distributed ZnO nanowire arrays for selective detection

Shell layers of 90 nm SnO<sub>2</sub>, In<sub>2</sub>O<sub>3</sub>, and WO<sub>3</sub> were sputtered in a Lesker PVD75 system with a deposition rate range of 0.2~0.5 Angstrom/s at room temperature.

A metal mask was employed to insure selective deposition in the process. Finally, the bottom and top electrodes connecting the nanowire arrays were prepared by microfabrication processes [71]. The structures and compositions were characterized by FESEM equipped x-ray energy dispersive spectroscopy (EDS).

### 2.1.2 Patterned grown well-aligned ZnO nanowire arrays

Schematics of fabrication procedures for well-aligned 3D sensors are shown in Fig. 2.2 To grow well-aligned ZnO nanowire arrays, 1 x 1cm<sup>2</sup> GaN/Al<sub>2</sub>O<sub>3</sub> (0001) substrate was spin coated

by PMMA and then electron beam lithography (EBL) technique was employed to generate square patterns on the PMMA layer where the ZnO nanowire grew out. A slight oxygen plasma cleaning (30 W, 30 seconds) was used to improve the wetting of nutrition solution on the PMMA layer. Hydrothermal growth was conducted after the EBL process. Furthermore, considering the nanowire arrays may affect the sensing properties of the devices, the nanowire arrays were obtained with different spacings and lengths by tuning the growth conditions.

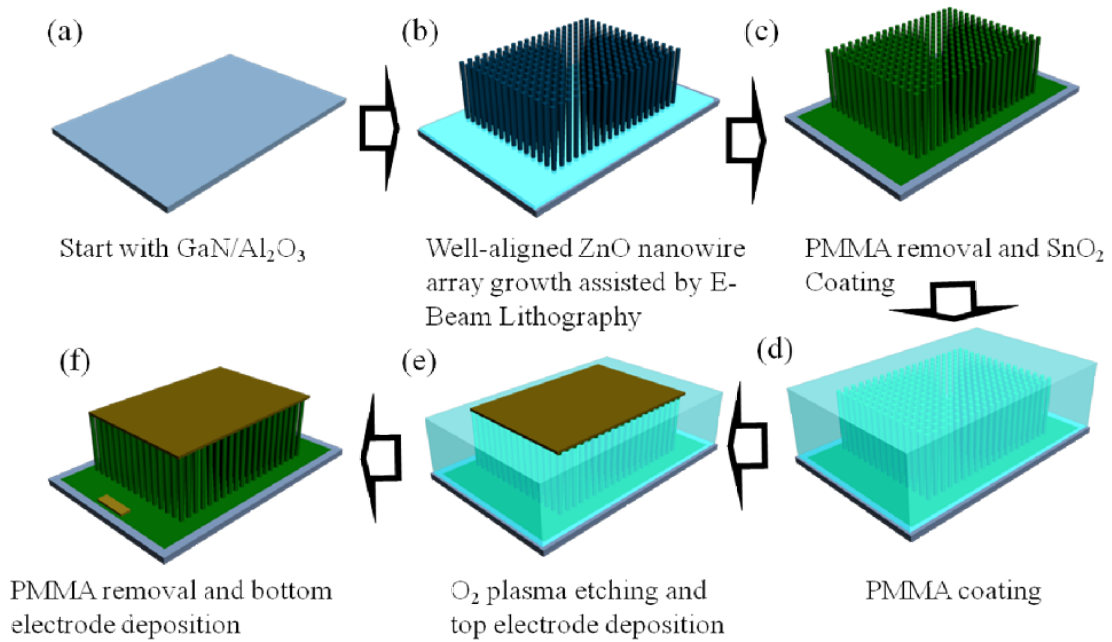


Figure 2.2 Schematic diagrams showing the procedures of 3-D gas sensor on patterned well-aligned ZnO nanowire arrays

Shell layers of 90 nm SnO<sub>2</sub> were sputtered onto the nanowire surfaces by a Lesker PVD75 system with a deposition rate range of 0.2~0.5 Angstrom/s at room temperature.

Though this method is good for the study on sensing performance of 3D nanowire arrays, the size of well aligned ZnO nanowire arrays are restricted by EBL capability, and further, the complexity of EBL also limited the yield of device fabrication.

## 2.2 Results and Discussion

### 2.2.1 Wafer size random-distributed ZnO nanowire arrays

Fig.2.3 (a, b) provides FESEM images of as grown ZnO nanowire arrays by hydrothermal method. The pristine ZnO nanowires are with 100 ~ 400 nm diameters and 6 $\mu$ m lengths. All of the nanowires are normal to the GaN/Al<sub>2</sub>O<sub>3</sub> (0001) substrate due to epitaxial growth.

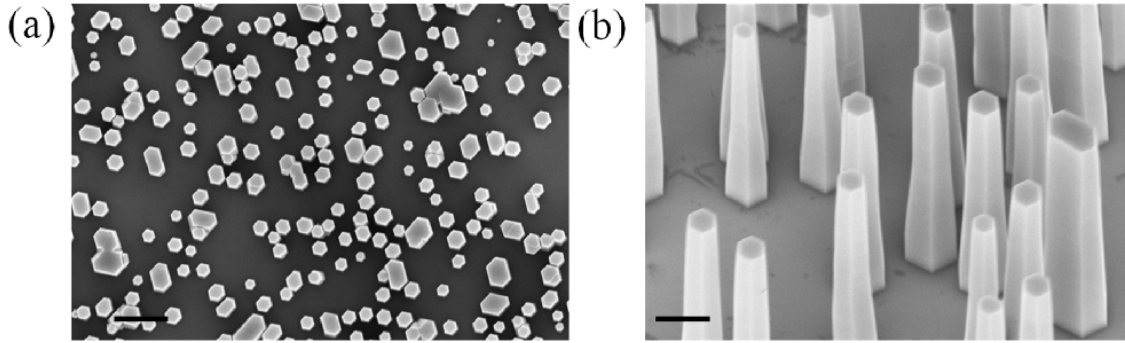


Figure 2.3 FESEM images of wafer size random-distributed nanowire arrays on GaN/Al<sub>2</sub>O<sub>3</sub> substrate. (a) Top view; (b) View by 30° tilting. (Scale bar is 1 $\mu$ m.)

Fig.2.4 (a, b, c) shows FESEM and EDS characterization on the nanowire arrays after different metal oxide coatings of SnO<sub>2</sub>, In<sub>2</sub>O<sub>3</sub>, and WO<sub>3</sub>. From the pictures, we can confirm that different metal oxides have been successfully coated on ZnO nanowire arrays from the roughness change of the nanowires and EDS results. In this experiment, all of metal oxides were coated by sputtering, since sputtering can generate uniform film because the thermalization and diffusion of sputtered species caused by the argon gases. In future, pulse laser deposition (PLD) will be investigated, because it is easy to form films with stoichiometry and an efficient way to yield single crystal films due to its high energy nature.

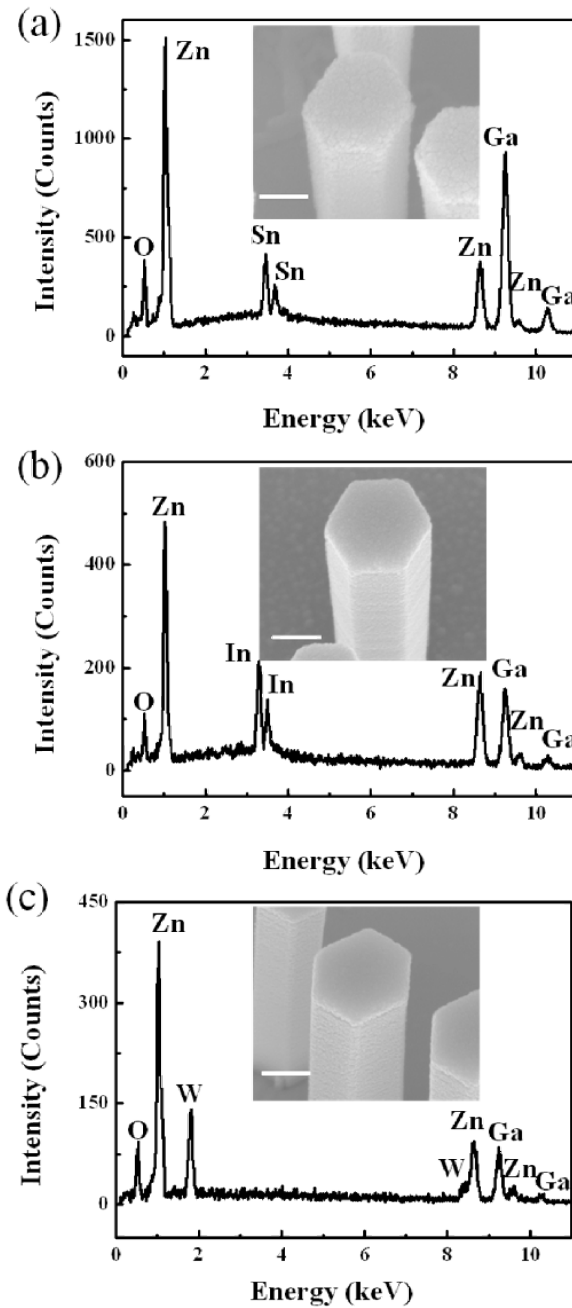


Figure 2.4 FESEM images and EDS analyses on random-distributed ZnO nanowire arrays with different metal oxide coatings. (a) SnO<sub>2</sub> coated ZnO nanowire arrays; (b) In<sub>2</sub>O<sub>3</sub> coated ZnO nanowire arrays; (c) WO<sub>3</sub> coated ZnO nanowire arrays. (Scale bar is 200nm.)

After different metal oxides' coating, I-V characteristics were obtained when the sensor arrays (ZnO/SnO<sub>2</sub>, ZnO/In<sub>2</sub>O<sub>3</sub>, and ZnO/WO<sub>3</sub>) were loaded into testing systems. The linear I-V plots in

Fig.2.5 indicate that the contact between the electrodes and nanowires are all ohmic. The resistances of all three core shell sensor arrays are in the same level  $\sim 10^6\Omega$ .

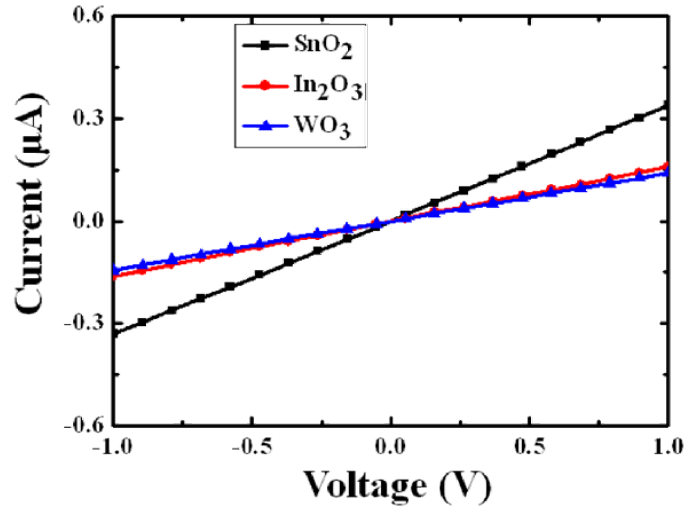


Figure 2.5 I-V curves for random-distributed nanowire arrays coated by different metal oxides.

After the basic I-V measurement, the conductances of the sensors were monitored simultaneously when the air-diluted testing gases with serial concentrations were introduced into the testing cells sequentially.

The exact fundamental mechanisms that cause a gas response are still controversial, but the sensing responses of metal oxide conductometric gas sensors can be explained by the processes of oxygen absorption and desorption on the metal oxide surfaces which is shown in Fig. 2.6 [72].

Trapping of electrons at adsorbed molecules and band bending induced by these charged molecules are responsible for a change in conductivity. When O<sub>2</sub> molecules are adsorbed on the surface of n-type metal oxides, they would extract electrons from the conduction band  $E_c$  and trap the electrons at the surface in the form of oxygen ions (O<sup>-</sup>, O<sup>2-</sup>, O<sub>2</sub><sup>-</sup>, etc.), which will lead a band bending and an charge depletion layer ( $L_D$ ). It can be described by

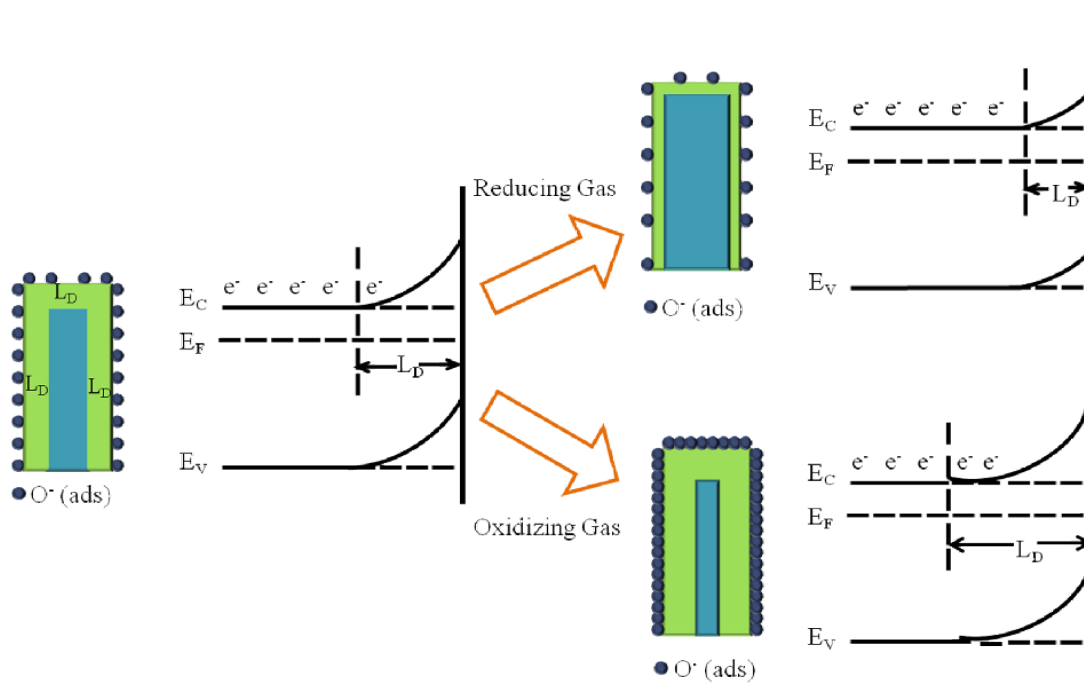
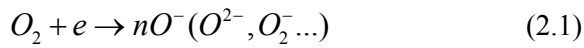
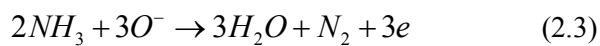


Figure 2.6 Diagram for mechanism of n-type metal oxide sensing responses.



The negative charge trapped in these oxygen species causes an upward band bending which results in a reduced conductivity compared to the flat band situation.

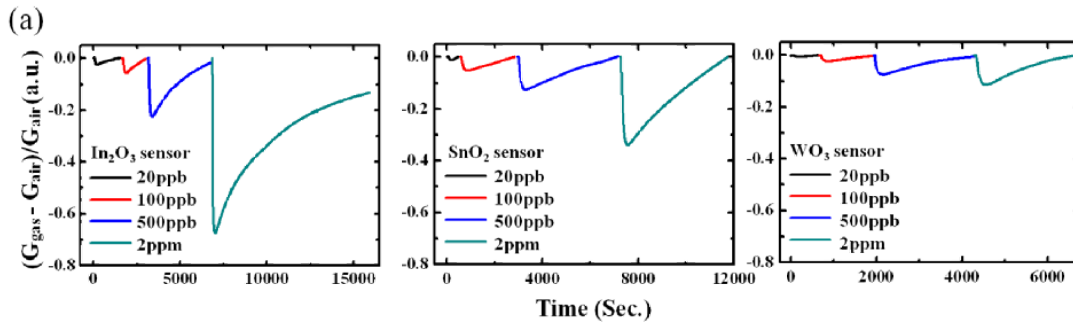
Reducing gases (H<sub>2</sub>S, NH<sub>3</sub>, CO, and H<sub>2</sub>) can react with these oxygen species, reverse the band bending and release the electrons back to the n-type metal oxides, leading to an increased conductivity. As described by



On contrary, oxidizing gases like NO<sub>2</sub> would decrease the device conductance. As described by



The sensing responses to air-diluted NO<sub>2</sub>, H<sub>2</sub>S, H<sub>2</sub>, CO, and NH<sub>3</sub> were tested with different concentrations at room-temperature, and all sensing responses which is defined by  $(G_{\text{gas}} - G_{\text{air}}) / G_{\text{air}}$  are plotted in Fig.2.7 (a-e). The devices showed high sensitivity to all five gases at room temperature. Especially to NO<sub>2</sub> and H<sub>2</sub>S, the lowest detection concentrations we reached are as low as 20 ppb and 50 ppb, respectively. H<sub>2</sub> and CO are generally difficult to be detected at room temperature by metal oxide conductometric sensors, but our devices detected air-diluted H<sub>2</sub> and CO at room temperature down to ppm level, which can be ascribed to the large surface area of the nanowire arrays. Moreover, the response speed of our sensors (duration from gas injection to 90% of sensing response) are pretty fast which were estimated to be about 3~5 mins. Compared with our group's previous sensor work based on monoclinic WO<sub>3</sub> array [9], WO<sub>3</sub>/ZnO core shell arrays in this experiment exhibited more promising properties, such as more sensitive to NO<sub>2</sub>, low energy consumption (whole process at room temperature), and so on. The better performance could be attributed to two reasons: (1) all of WO<sub>3</sub>/ZnO core shell nanowires are normal to the substrate and have much bigger space between each other which leads to better gas diffusion; (2) The lengths of WO<sub>3</sub>/ZnO core shell nanowires are even and larger which results in larger sensing area and better contact between all nanowires and top electrode.



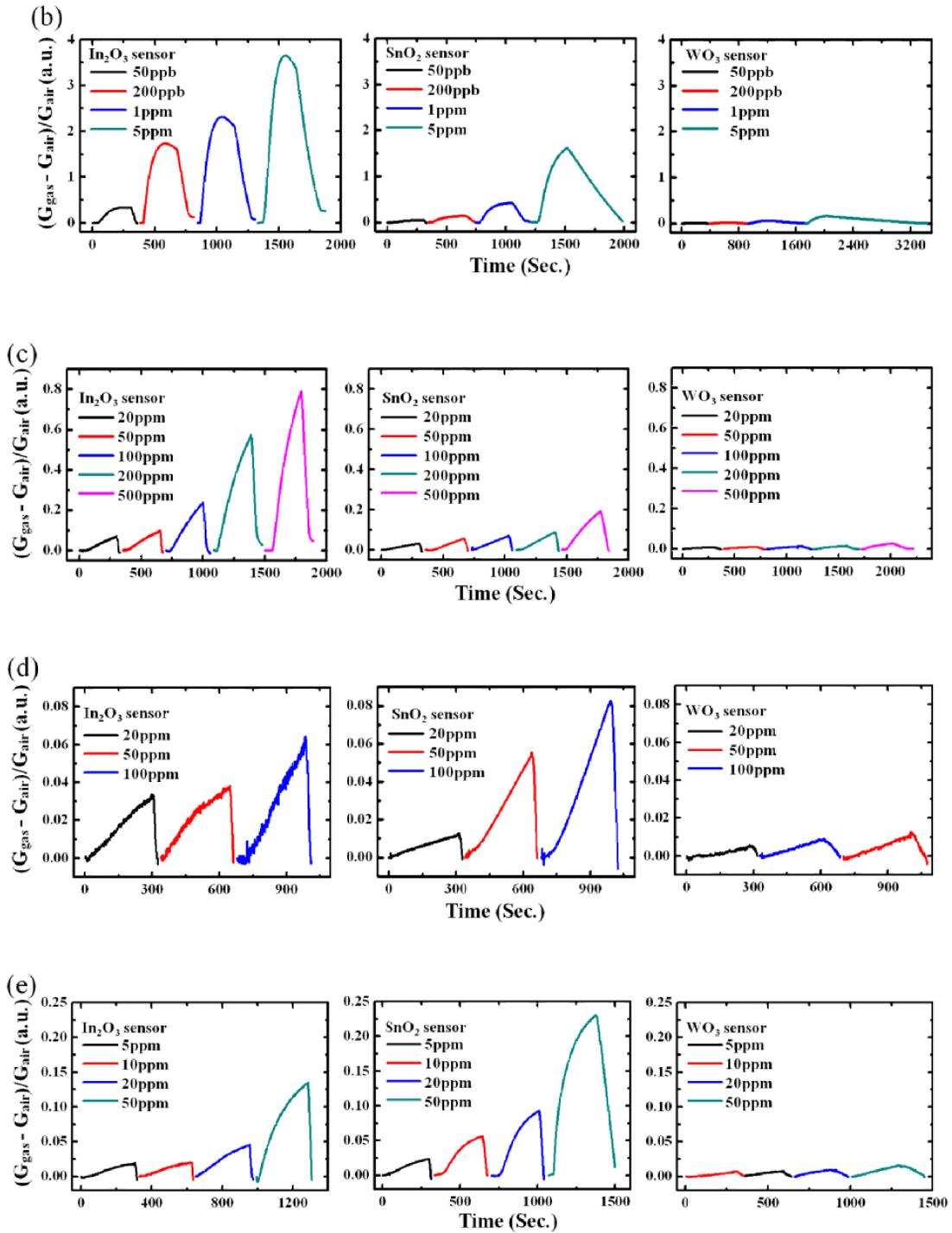


Figure 2.7 Sensing responses to different gases at room temperature (a)  $\text{NO}_2$ ; (b)  $\text{H}_2\text{S}$ ; (c)  $\text{H}_2$ ; (d)  $\text{CO}$ ; (e)  $\text{NH}_3$ . (Random-distributed nanowire array sensing devices)

From the plots in Fig.2.7, the oxidizing gas ( $\text{NO}_2$ ) could be easily distinguished from the other four reducing gases, since the negative response was detected to  $\text{NO}_2$  in Fig.2.7(a), while the other four gases showed positive responses in Fig. 7(b-e).

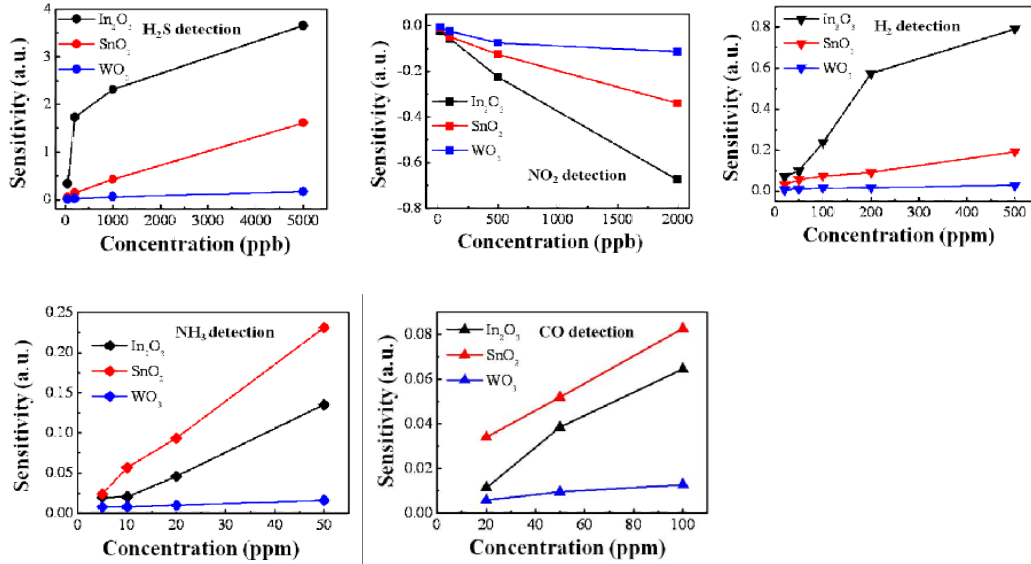


Figure 2.8 Sensing response comparisons to different gases at room temperature. (Random-distributed nanowire array sensing devices)

Fig.2.8 shows the sensing response comparison to different gases from three devices at room temperature. We could see  $\text{In}_2\text{O}_3$  device has best sensitivity to  $\text{H}_2\text{S}$ ,  $\text{NO}_2$ , and  $\text{H}_2$ , while  $\text{SnO}_2$  device has best response to  $\text{NH}_3$  and  $\text{CO}$ . The response differences are related to the intrinsic properties of the sensing materials.

To discriminate the other four gases, an efficient way is to employ statistical method to extract feature from the experiment datas. There are a number of widely known feature extraction methods such as Principal Component Analysis (PCA) and Linear Discriminant Analysis (LDA), and further improvements to these methods are still being made [73, 74]. Since PCA is a linear unsupervised method that requires no or little prior knowledge, and in most case, only response variables (response strength, speed) are needed, it was applied in our experiment.

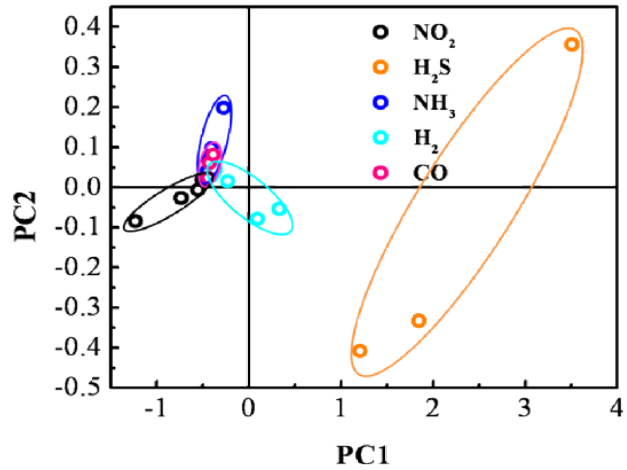


Figure 2.9 PCA analysis of sensing responses from the random-distributed sensor arrays.

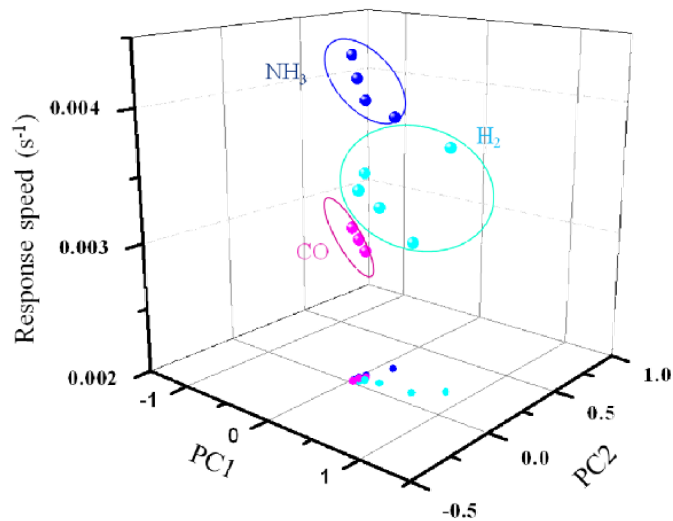


Figure 2.10 Plot of PCA data incorporated with sensing response speeds for discrimination of  $H_2$ , CO, and  $NH_3$ .

Fig.2.9 is the PCA analysis plot of sensing responses from the sensor arrays, by which  $H_2S$  is easily to be distinguished from the other gases. However, the other three gases ( $H_2$ , CO and  $NH_3$ ) are overlapped at low concentration region, which means it is difficult to distinguish them from the two dimensional PCA plot. As the gas sensors showed different sensing response speeds when exposed to  $H_2$ , CO and  $NH_3$ , it may be considered as additional major factor to increase the capability of gas discrimination. Fig.2.10 is the 3D plot of PCA incorporated with the response

speeds, from which three gases of H<sub>2</sub>, CO and NH<sub>3</sub> have been well distinguished. To discriminate more targeting gases, sensor arrays built with various materials are essential, which will be explored in future.

## 2.2.2 Patterned grown well-aligned ZnO nanowire arrays

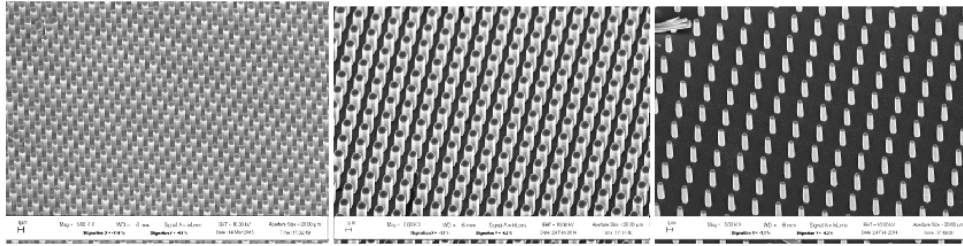


Figure 2.11 Patterned well-aligned nanowire arrays with different spacings

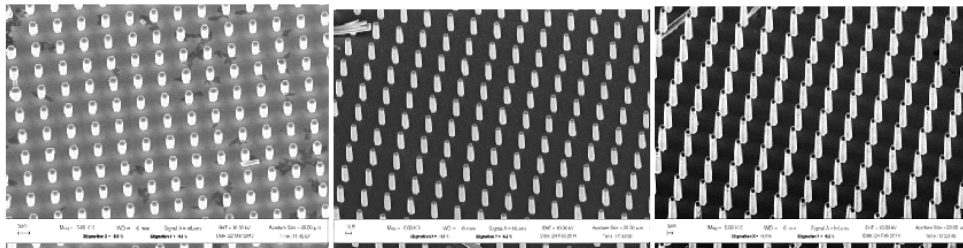


Figure 2.12 Patterned well-aligned nanowire arrays with different lengths

Fig.2.11 and Fig.2.12 are the FESEM images of as-grown ZnO nanowire arrays prepared by hydrothermal method combined with EBL technique. It is clearly shown that the growth positions of nanowires are well-defined by the EBL and the nanowires are all vertically grown due to epitaxial growth. Moreover the nanowire lengths and spacings are well controlled. In Fig.2.11, nanowire arrays have same lengths of 6 $\mu$ m but with different spacings of 1 $\mu$ m, 2  $\mu$ m and 3  $\mu$ m among (a)-(c), while nanowire arrays in Fig.2.12 have same spacings of 3 $\mu$ m but with different nanowire lengths of 3 $\mu$ m, 6 $\mu$ m, and 9 $\mu$ m among (a)-(c).

### 2.2.2.1 ZnO nanowire arrays with same lengths but different spacings

Fig.2.13 shows the sensing responses to air-diluted H<sub>2</sub>S with different concentrations at room temperature. The results demonstrated all the devices have pretty high sensitivity to H<sub>2</sub>S and could detect H<sub>2</sub>S at very low concentration of 20ppb, which can be ascribed to the large surface area and better gas diffusion in well-aligned nanowire arrays.

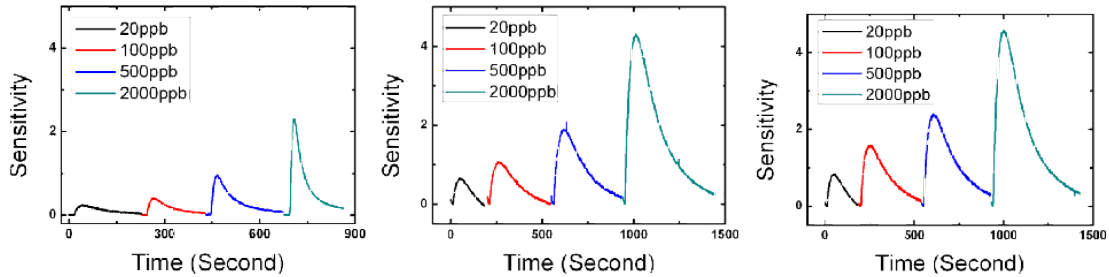


Figure 2.13 Sensing responses to H<sub>2</sub>S at room temperature (Different spacings)

To compare the sensing responses among different spacing arrays, we found it is big enhanced when the spacing was enlarged from 1 $\mu$ m to 2 $\mu$ m. That is because the spacing would directly affect the targeting gas diffusion and large spacing can help more nanowires react with the targeting gas which will lead to higher resistance change. However, only little enhancement could be seen when the spacing was increased from 2 $\mu$ m to 3 $\mu$ m. Therefore, we can see spacing is one of key factors for 3-D gas sensors and certain spacing could highly improve the gas sensor performance. For our system, the sensitivity could not be much improved by increasing the spacing after it is more than 2 $\mu$ m.

### 2.2.2.2 ZnO nanowire arrays with same spacings but different lengths

To further improve the sensitivity of the 3-D gas sensors, several devices were fabricated based on nanowire arrays with same spacings of 3 $\mu$ m but different lengths of 3 $\mu$ m, 6 $\mu$ m and 9 $\mu$ m, and

it is tested that the sensing responses to air-diluted H<sub>2</sub>S with different concentrations at room temperature which is shown in Fig.2.14.

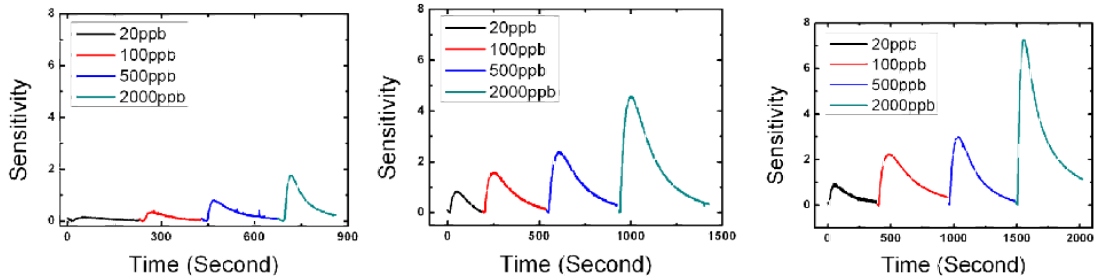


Figure 2.14 Sensing responses to H<sub>2</sub>S at room temperature (Different lengths)

All the devices are capable to detect H<sub>2</sub>S as low as 20ppb. From 3 $\mu$ m to 6 $\mu$ m lengths of the nanowire arrays, the sensitivities at all H<sub>2</sub>S concentrations have been greatly improved. The increase in sensitivity can be ascribed to two major factors: (1) longer nanowires enlarge the space between the top electrode and substrate which would enhance the diffusion of the targeting gas, (2) longer nanowires own more reaction surface than shorter ones. Compared 6 $\mu$ m with 9 $\mu$ m long nanowire arrays, the sensitivity is only highly improved at high H<sub>2</sub>S concentration, while no big improvement could be seen at low concentrations, because the quantities of gas molecules are limited at low concentrations. Therefore, lengths of nanowires are crucial to build highly sensitivity 3-D gas sensors and longer nanowires would improve the properties of the gas sensors.

## 2.4 Conclusion

An electronic nose system based on wafer size random-distributed ZnO nanowire arrays with different gas sensing metal oxide coatings has been demonstrated for gas discrimination of NO<sub>2</sub>, H<sub>2</sub>S, H<sub>2</sub>, NH<sub>3</sub>, and CO at room temperature assisted with principal components analysis (PCA) incorporated with sensing response speeds. The SnO<sub>2</sub>, In<sub>2</sub>O<sub>3</sub>, and WO<sub>3</sub> coated ZnO sensors showed responses to NO<sub>2</sub> and H<sub>2</sub>S with concentrations as low as 20 ppb and 50 ppb, respectively.

Our methods provide a promising way to adapt more metal oxide materials on the novel 3D prototype gas sensors.

Highly sensitive gas sensors base on patterned well-aligned nanowire arrays have been fabricated and all are capable to detect H<sub>2</sub>S as low as 20ppb. Several key factors, such as nanowire lengths and spacings, have been investigated to further improve the performance of the 3-D gas sensors.

## Chapter 3 PEDOT:PSS/ZnO nanowire arrays VOC sensor

Even though conducting polymer gases sensors are good at detecting VOCs, but they are suffering from long-time instability and irreversibility [75]. Long-time instability is a main drawback affecting the application of the conducting polymer sensors. Especially, if the conducting polymer gas sensors are stored in air, their performances would degrade dramatically in a relatively long time due to de-doping of conducting polymers. Meanwhile, oxygen may also cause degeneration of some conducting polymers. Another issue is the irreversibility of conducting polymer sensors. The response gradually falls down after being cyclic exposed to analytes.

To overcome these drawbacks, it may be a good way to incorporate second component, such as carbon nanotubes, metal clusters and metal oxides, into conducting polymers. Certain second components may be helpful to improve the mechanical property or protect sensing film as well as to improve the properties of sensing film due to facilitate electron or proton transfer or directly interact with analytes [76].

### 3.1 Experiment

As reported in chapter 2, 3D ZnO nanowire arrays were grown on GaN substrate by hydrothermal method. PEDOT:PSS was spin-coated on 3D ZnO nanowire array template. And then, the substrate was cured at 100<sup>0</sup>C for 30 minutes in the oven. Au electrodes are coated on two sides of substrates. The schematics are shown in Fig.3.1. We could see the two electrodes are coated on PEDOT:PSS thin film, therefore, ZnO nanowire arrays are only template, which provides the large absorption area for gas molecules. Fig.3.2 shows the molecular structure of PEDOT:PSS in which the  $\pi$ -conjugated system is responsible for the hole transport in PEDOT [77].

When PEDOT:PSS conductive polymer exposes in reducing gases, such as acetone, ethanol and methanol, The electrons transferred between these reducing gases and PEDOT:PSS leads to the formation of neutral polymer chains and results in the decrease of charge carrier density, which decreases the conductivity of PEDOT:PSS. Moreover, since PEDOT:PSS is porous structure, the gas absorption will cause the polymer swelling which may affect the conductivity of PEDOT:PSS [78].

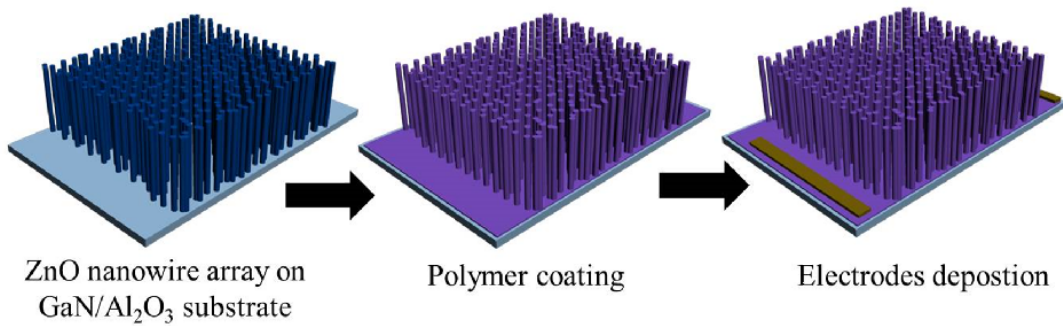


Figure 3.1 Schematics for fabrication PEDOT:PSS/ZnO array gas sensors.

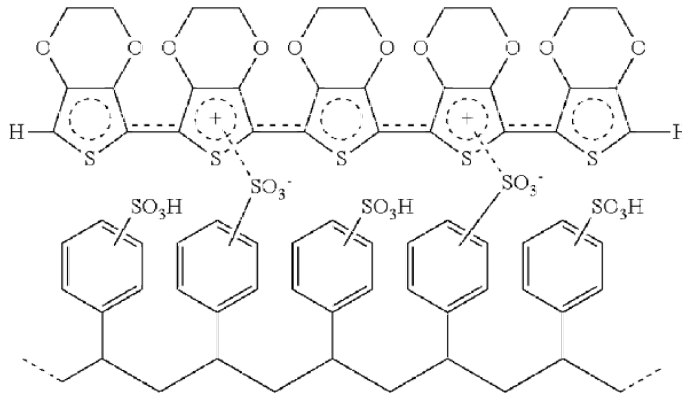


Figure 3.2 Molecular structure of PEDOT:PSS.

As mentioned above, the big issues for conducting polymer gas sensors are instable and irreversible. To overcome these drawback, Metal oxide nanoparticles are added to PEDOT:PSS solution [23]. For well dispersion of metal oxide nanowires, the mixed solution was stirred for 5 hours before coating on ZnO nanowire arrays. In this experiment, several samples are prepared of 0.1mg SnO<sub>2</sub> nanoparticles, 0.2mg SnO<sub>2</sub> nanoparticles and 0.5mg SnO<sub>2</sub> nanoparticles in 5ml

PEDOT:PSS solution respectively. Since  $\text{SnO}_2$  is well known n-type semiconductor, the n type  $\text{SnO}_2$  nanoparticles will trap holes at the interface with PEDOT:PSS polymer.

### 3.2 Results and discussions

Fig.3.3 are the IV curves for devices one time spin-coated by pure PEDOT:PSS(sample1), 0.1mg  $\text{SnO}_2$ /5ml PEDOT:PSS(sample2), 0.2mg  $\text{SnO}_2$ /5ml PEDOT:PSS(sample3) and 0.5mg  $\text{SnO}_2$ /5ml PEDOT:PSS(sample 4). We could find the device coated by pure PEDOT:PSS has biggest current, which means lowest resistance. With the addition of  $\text{SnO}_2$  nanoparticles, more  $\text{SnO}_2$  caused lower current, which means higher resistance. When the  $\text{SnO}_2$  disperses in PEDOT:PSS solution, some charge carrier (holes) in PEDOT:PSS will be trapped by n type  $\text{SnO}_2$  leading to higher resistance. More  $\text{SnO}_2$  addition will cause even higher resistance of the device.

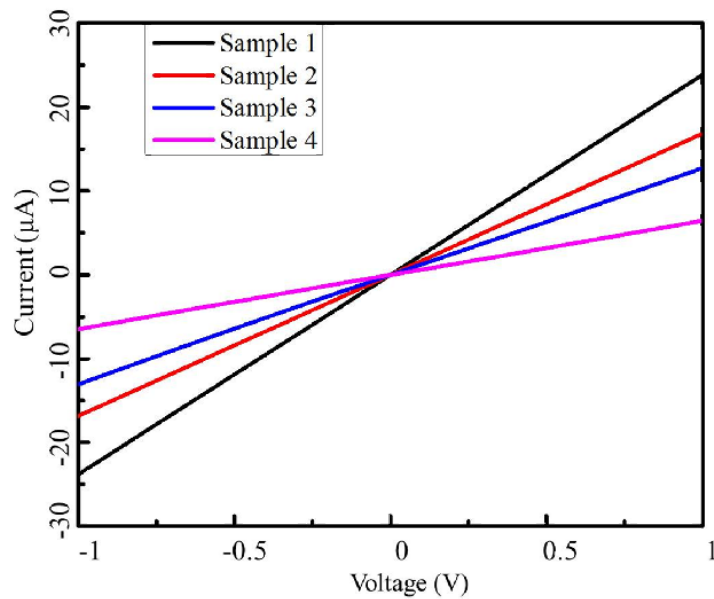


Figure 3.3 IV curves for four different devices.

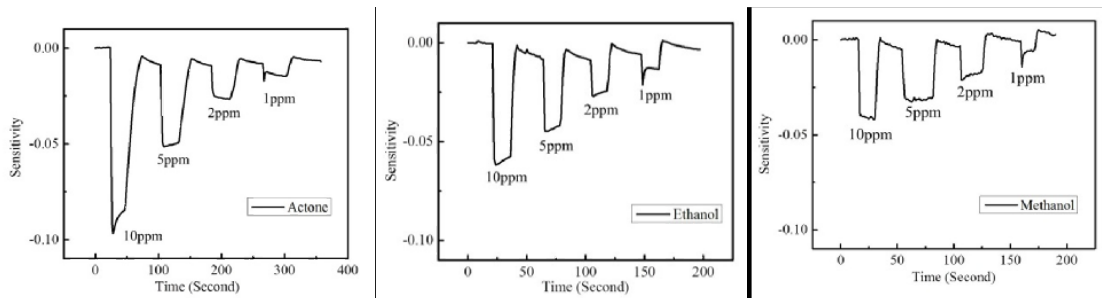


Figure 3.4 Sensing responses to actone, ethanol and methanol at various concentrations of device coated by pure PEDOT:PSS.

Fig.3.4 shows the Sensing response to actone, ethanol and methanol at various concentrations (10ppm, 5ppm, 2ppm, 1ppm) of device coated by pure PEDOT:PSS. The device coated by pure PEDOT:PSS has good sensitivity to actone, ethanol and methanol, and the device has good reversibility, even at relatively high concentration of 10ppm. That may be because of the extremely large surface area provided by 3D ZnO nanowire arrays. For all the testing process, it only took several seconds for the device to to response and recover.

The sensing mechanisms of conducting polymer gas sensors are multi-forms for different analytes and different active materials [79]. One is chemical reactions between analytes and conducting polymers. Chemical reactions would easily change the doping levels of conducting polymer which is associated with the conductance of the polymer. The other one is physical interactions between analytes and the sensing polymers, involving absorbing or swelling the polymer.

When the PEDOT:PSS film is exposed to the reducing gases of acetone, ethanol and methanol, the hole-conducting PEDOT:PSS-rich islands on the film surface will interact with the electron-donating analyte [80]. The PEDOT:PSS chains accept electrons from the adsorbed gas molecules, and thus the delocalization degree of conjugated electrons along the PEDOT:PSS backbones increases with the density drop of charge carriers which transfer along the polymer chains. The high yield of the neutral PEDOT:PSS backbones and rapid decrease of charge carriers, induce a

conductivity drop of PEDOT:PSS film. Conversely, the absorbed gas molecules will be separated from the PEDOT:PSS film by air flow. The desorption of the analyte molecules will induce the electron depletion in the PEDOT:PSS chains, leading to the rapid increase of the charge carriers (holes) in the polymer matrix. Therefore, the conductivity of the sensor will recover toward its initial value. On the other hand, the gas sensing mechanism is most probably due to the swelling of the polymer by uptake of the analyte molecules. The swelling causes an increase in distance between PEDOT:PSS chains and thus the electron hopping process becomes more difficult [81]. Hence, the conductivity of the polymer decreases. The swelling of the polymer can disappear after the purge by air flow, leading to the recovery of the polymer composite sensor.

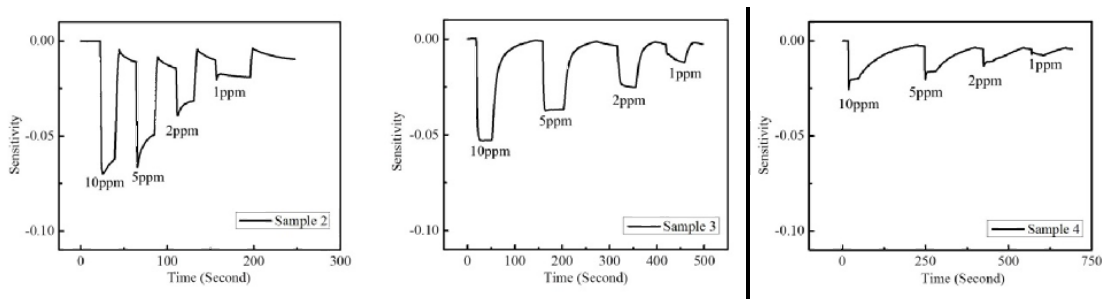


Figure 3.5 Sensing responses to actone at various concentrations of devices - sample2, sample3, and sample4.

Fig.3.5 shows the Sensing responses to actone at various concentrations (10ppm, 5ppm, 2ppm, 1ppm) of devices - sample2, sample3, and sample4. All the devices are capable to detect actone to 1ppm and have short response time. However, compared with device coated with pure PEDOT:PSS, the devices with addition  $\text{SnO}_2$  showed worse sensitivity to acetone at same concentration. It may be because the p-n junction trapped carrier charge of PEDOT:PSS which lower the reaction probability between PEDOT:PSS and actone. More  $\text{SnO}_2$  addition will kill more sensitivity. Moreover, with the addition of  $\text{SnO}_2$ , the PEDOT:PSS film becomes less porous, so the conductivity change caused by swell effect will be reduced. That may also be related to the worse sensitivity. With more  $\text{SnO}_2$  nanoparticles, the recovery time becomes longer. That may

also be associated with the process of trapping and releasing holes by SnO<sub>2</sub> particles. However, a little longer recovery time may be helpful for polymer gas sensor, since that means it would be violated by air flow. It may provide a way for more stabilized polymer gas sensors.

### **3.3 Conclusions**

PEDOT:PSS coated ZnO nanowire arrays gas sensors have good sensitivity, fast response and recover to acetone, ethanol and methanol. With SnO<sub>2</sub> addition, some charge carrier (holes) in PEDOT:PSS will be trapped by n type SnO<sub>2</sub> leading to higher resistance, which will influence the performance of devices on sensitivity and recovery time. However, it may provide a good way to adjust the properties of PEDOT:PSS conducting polymer for fabrication more stabilized gas sensor.

## Chapter 4 Low voltage air ionization sensor with ZnO nano-rods electrode

Gas ionization is the fundamental mechanism of gas sensor based on ionization (GSBI). It was reported that GSBI has good selectivity because the ionization energies of gases are one of their fingerprinting characters. Each gas has a unique electrical breakdown voltage at constant temperature and pressure. As being reviewed in literatures, traditional GSBI used in chromatograph and mass spectrograph cannot be used on site because of the high power consumption, huge structure and risky high operation voltage which is the main issue. To overcome these drawbacks of traditional GSBI, one possible way is to explore new materials which could generate relatively high electric field at low voltage [82].

With the development of nano-material research, people found high electric fields could be generated at tips of nano-tubes and nano-rods electrodes, which is leading to build one new type GSBI with nano-material electrodes. The reported nano-materials include carbon nano-tubes, ZnO nano-rods, gold nano-rods and silver nano-rods. With these nano-material electrodes, the gas electrical breakdown voltage ( $V_{EB}$ ) has been realized at relatively low level and been reduced several folds compared with traditional plane electrodes. Moreover, this new type GSBI was proved to be reversible quickly as no chemical absorption is involved [83].

It was reported that electric field enhancement is highly related to the morphology of tips. Among plane, tapered, and abruptly sharp tips, the abruptly sharp tips has the highest electric field enhancement factor. As a widely studied material, the tip morphology of ZnO nano-rods could be well controlled. Additionally, as an electrode material of GSBI, it was confirmed that ZnO nano-rods have better stability and anti-oxidation behavior than carbon nano-tubes [29].

To further reduce gas  $V_{EB}$ , both metal decoration and narrowing down electrode distance have been investigated. Although gas  $V_{EB}$  has been decreased by these methods, the voltage is still much higher than a safe voltage (the safe operation criteria voltage is below 36 V). For the ZnO

nano-rods electrode, the  $V_{EB}$  of air is as high as 335 V when the distance between two electrodes is reduced to 25  $\mu\text{m}$ . For the capacitance structure gas-gap device, it is very hard to further decrease the electrodes distance. Also, sole Pd decoration only could decrease the  $V_{EB}$  of air from 363 V to 341 V. Therefore, it is difficult to reduce the  $V_{EB}$  below the safe operation criteria by capping sole metal or decreasing electrode distance [84].

Another effective way to reduce the  $V_{EB}$  is to control the motion of electron by magnetic field. It is interesting that both longitudinal (parallel to electrical field) and transverse (perpendicular to electrical field) magnetic field are facilitating gas electrical breakdown on plane parallel electrodes with large separation distance (distance is about several centimeters). The devices based on nano-material electrodes may be beneficial under magnetic field. To our best knowledge, no report has been published on gas ionization by ZnO nano-rods electrodes under magnetic field. In this paper we studied the metal decoration and magnetic field effect on reducing  $V_{EB}$  for ZnO nano-rods electrodes [85].

## 4.1 Experiment

ZnO nano-rods fabrication process was reported by Xiao et al. The ZnO nano-rod arrays were grown on Si substrates in a conventional horizontal tube furnace with a quartz tube. The substrate is n type [100] Si wafers with top 300 nm  $\text{SiO}_2$  layer [86]. First of all, the substrates were ultrasonically cleaned in acetone, IPA, and distilled water and then dried by nitrogen flow. After being carefully cleaned, 30 nm gold film was sputtered on Si substrates by Cressington 308R thin film coating system, which will be served as anode electrode. The film thickness was monitored by a quartz oscillator. The base pressure of sputter chamber is  $1 \times 10^{-7}$  bar, and the working pressure is 0.02 bar. Secondly, ZnO seeds layer was drop coated on the gold film. Zinc acetate (Fisher scientific) ethanol solution of 0.015 M was prepared. 20  $\mu\text{l}$  solution was dropped onto the surface of gold film. After waiting for 30 seconds, the substrate was dried by nitrogen flow. This

process was repeated for six cycles. Thirdly, 0.5 grams Zn powder (Damon 5918J25) was loaded on the center of an alumina boat and served as the source material. Several substrates with gold film and seeds layer were faceddown put over the source material about 2-3 mm and different distances to the center of boat. The alumina boat with both the source material and the substrates was pushed to the center of the quartz tube, which would be pumped down to a pressure of 8 Torr with a mechanical pump. Argon gas was then introduced into the tube as a carrier gas with a flux of 50 standard cubic centimeters per minute (SCCM). The furnace temperature was subsequently increased from room temperature to 550°C within 50 minutes. During the heating up process, oxygen gas was introduced at a flux of 5 SCCM when the temperature of furnace reached 450°C. The temperature of furnace was maintained at 550°C for 30 min. Thereafter, the furnace temperature was decreased from 550°C to 450°C within 40 minutes, and then the furnace was turned off and naturally cooled down to room temperature. The crystal structure of the sample was characterized by Philips X'pert MPD X-ray diffraction (XRD). The morphology of the sample was measured with a Carl Zeiss LEO 1530VP field emission scanning electron microscope (FESEM) and a JEOL 2010 transmission electron microscope (TEM). The composition analyses were conducted by the X-ray energy dispersive spectroscopy (EDS) equipped on TEM.

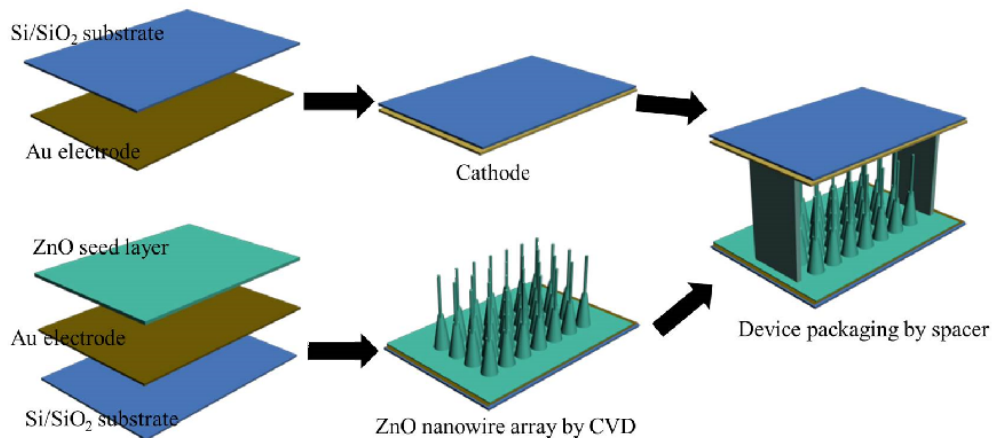


Figure 4.1 Schematics of ionization device fabrication

To fabricate the device, ZnO nano-rod arrays were served as the anode and the Si/SiO<sub>2</sub> substrate coated with 30 nm gold films was used as the cathode. The distance was fixed at 200 μm between anode and cathode. The magnetic field generated by a permanent magnet was measured by Lakeshore 450 Gaussmeter. The IV curves of devices were tested by Keithley 2400 source meter. Fig.4.1 is the schematics of 3D ZnO nanowire arrays ionization device fabrication. Insulate separator are sandwiched by Au coated Si cathode and ZnO nanowire arrays anode.

## 4.2 Results and discussion

A typical morphology of ZnO nano-rod arrays with abrupt sharp tips is shown in Fig.4.2 which has the low and high magnification FESEM images of 30° tilt view. The wafer-size nanorod arrays are well aligned and normal to the substrates. We believe the ZnO seed layer not only contributes to perpendicular growth of nano-rod arrays, but also protects the gold film anode electrode. Since there are not metallic particles observed on nano-rod tips, the growth of the ZnO nano-rod arrays could be governed by a self-catalytic mechanism.

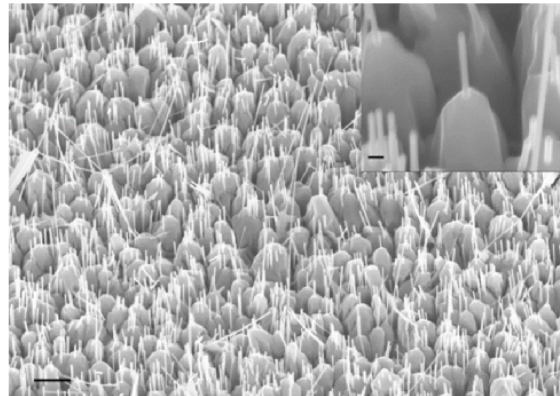


Figure 4.2 ZnO nano-rod arrays FESEM images of 30° tilt (scale bar is 1 μm in low magnification image, and 100 nm in inserted high magnification image).

During heating process, Zn vapor would condense on the ZnO seed layer surface and then be oxidized by the O<sub>2</sub> to form ZnO. The ZnO would form as solid particles which would act as

nuclei and trigger further growth of the nano-rod, because ZnO had a much higher melting point than Zn. The insert image clearly shows the nano-rod has two-stage geometrical configuration with a large cylinder-like base with diameter of about 600 nm and abrupt sharp tips with a diameter of about 50 nm, indicating growth process has been divided into two stages by the growth temperature change.

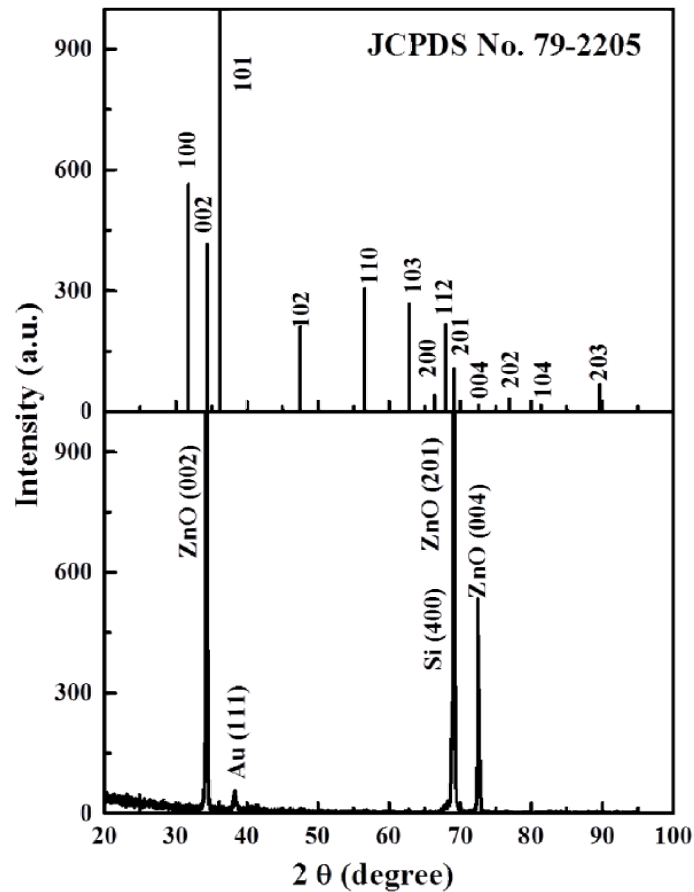


Figure 4.3 XRD pattern of pristine ZnO nano-rod arrays

Fig.4.3 shows the XRD pattern of pristine ZnO nano-rod arrays. The obtained ZnO nano-rod arrays have the hexagonal structure confirmed by XRD measurement. The diffraction peaks located at  $34.31^\circ$  and  $72.47^\circ$  are indexed respectively as (002) and (004) of ZnO (JCPDS No. 79-2205). The (002) diffraction peak is the strongest reflection, indicating the (002) is the

preferential growth plane of the ZnO nano-rods. The lattice constant  $c$  is calculated to be 0.522 nm. The peak at  $38.23^\circ$  is indexed as (111) diffraction from gold (JCPDS No.04-0784). The diffraction peaks located at  $69.04^\circ$  is indexed as (004) of Si (JCPDS No. 75-0590).

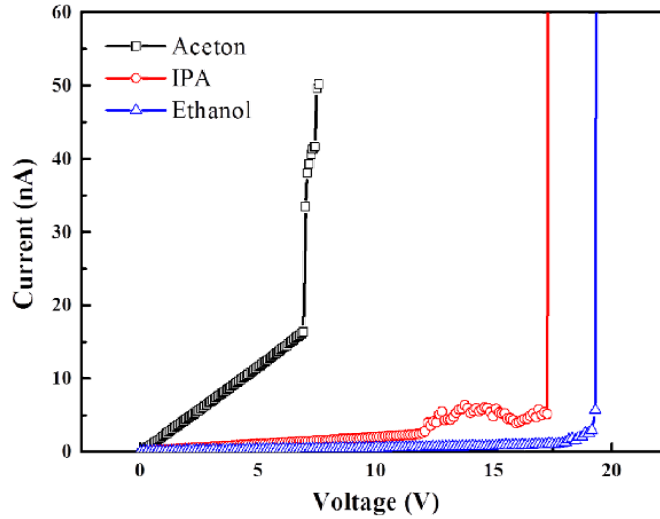


Figure 4.4 Ionization detection by pristine ZnO nano-rod array device in different atmosphere (6% Acetone, IPA and Ethanol)

The devices fabricated by pristine ZnO nano-rod arrays were employed to detect 6% acetone, IPA, and ethanol, which results is shown in Fig.4.4. The  $V_{EB}$  for three different gases are 6.9V, 17.3V and 19.3V, respectively, which is distinct for each gas. Such low  $V_{EB}$  shows the great potential of ZnO nano-rod arrays with abrupt sharp tips. The excellent performance is because the field emission on nanorods with abrupt sharp tips could be well concentrated and strengthened in the tip region leading to much better field enhancement ability. Even more, the relative low density of the abrupt sharp tips would improve the field emission, since the electrostatic shielding by the adjacent nanotips would get stronger when the density becomes higher. Therefore, the emissions from the primary cylinder-like base section and any other blunt position are eliminated efficiently and the electrostatic shielding effect can also be efficiently suppressed due to the good localization of the field distribution around the tip morphology. However, the device cannot

ionize air even though the applied voltage was elevated to 210 V, because  $V_{EB}$  is mainly determined the ionization energy of gas, and the ionization energies of oxygen and nitrogen (main contents of air) are much higher than these organic gases. The ionization energies of oxygen and nitrogen are 12.06 and 15.58 eV, while the ionization energies of acetone, IPA, ethanol are 9.69, 10.12, and 10.62 eV, respectively.

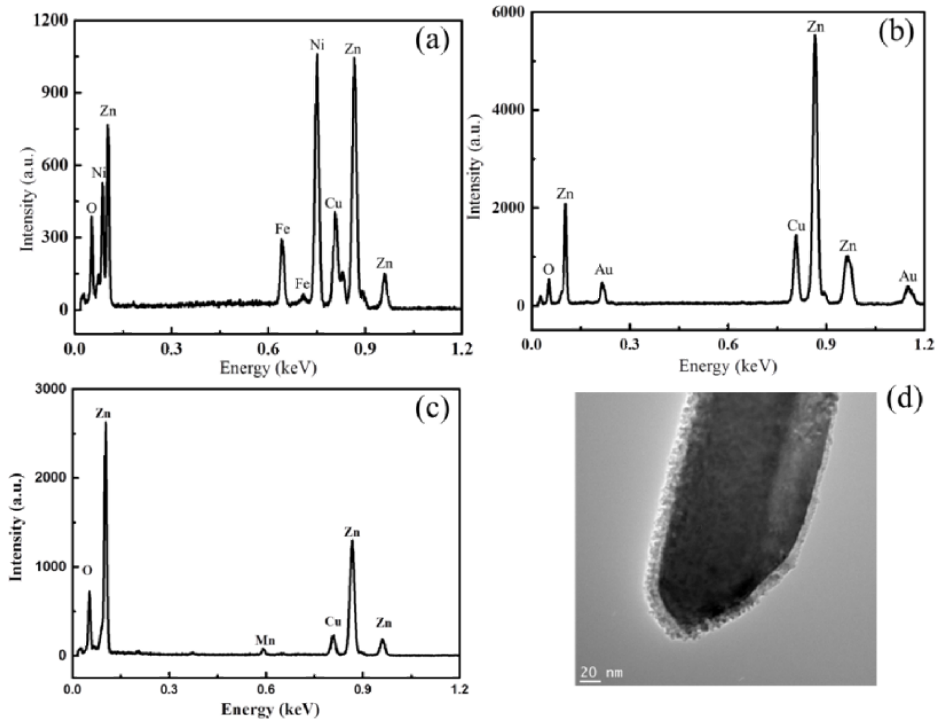


Figure 4.5 EDS for ZnO decorated by different metals (a) 15nm  $Fe_{19}Ni_{81}$  (b) 15nm Au (c) 15nm Mn. (d) TEM image for ZnO nanowires coated with 15nm Mn.

In order to ionize gas with high ionization energy, 15nm  $Fe_{19}Ni_{81}$ , Au and Mn were separately sputtered on ZnO nano-rod arrays to improve the performance of the devices, since tiny protuberances would be created on the surface of nano-rods after sputtering coating thin layer metals on ZnO nano-rod arrays, and the tiny protuberances could generate higher nonlinear electric field and thus decrease the electrical breakdown voltage of gases [84]. However, it is still hard to decrease air  $V_{EB}$  to a safe operation voltage only by metal decoration, because the

collision probability is low between electron and molecule in the field enhanced region due to the mean free path of electron in air which is about 0.5  $\mu\text{m}$  much larger than the field enhanced region of nano-tips. As we know, magnetic field could confine the motion electrons and decrease the free path of electrons [87]. Therefore, we also employed magnetic field to increase the collision frequency between electron and molecule in the field enhanced region.

Fig.4.5 exhibits the EDS for ZnO nano-rod arrays coated by different metals. Through Fig.4.5 (a), 5(b) and 5(c), we could clear see the peaks corresponding to the metals of  $\text{Fe}_{19}\text{Ni}_{81}$ , Au and Mn. Cu peaks are from the TEM grids. Fig.4.5(d) is the TEM image for ZnO nanowires coated by 15nm Mn. We could see the ZnO nanowires are well coated by the uniform Mn film.

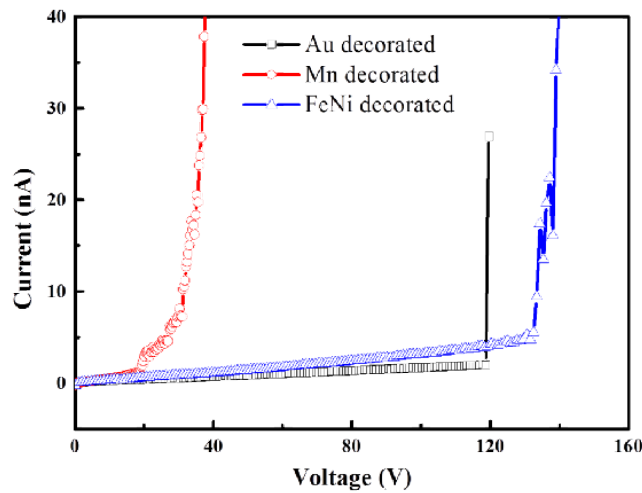


Figure 4.6 Air ionization for various metal decorated ZnO nano-rods under 6000 Gs transverse magnetic field

Fig.4.6 shows the ionization of air by devices with 15 nm of Au,  $\text{Fe}_{19}\text{Ni}_{81}$  and Mn decoration under 6000Gs transverse magnetic field (A transverse magnetic field exerts action on the motion of electrons, which makes the gyro-motion of electrons, reduces the path of electrons and increases the number of collision and ionization coefficient). All three devices could reduce air breakdown voltage lower than 210V. The performance has been much improved compared with

pristine nano-rod array device. Especially, the device decorated by Mn has lowest air breakdown voltage which is around 20V. The excellent performance benefits from the enhancement of the field emission by metal decoration and increasing of collision frequency between electrons and gas molecules by transverse magnetic field.

Fig.4.7 shows the air ionization by devices with various thickness (5nm, 10nm, and 15nm) Mn decorations under 6000Gs transverse magnetic field. The 5nm Mn coating device has lowest breakdown voltage to air, and the breakdown voltage to air increases with increasing of Mn thickness, because thinner coating would form more protuberance islands on the surface of nano-rod, while 15nm Mn coating forms thin film, indicating the protuberance islands could further enhance the field emission.

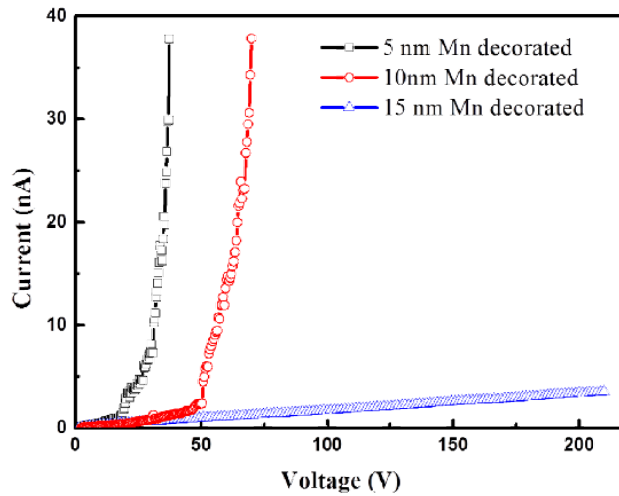


Figure 4.7 Air ionization for ZnO nano-rod electrode decorated with various Mn thicknesses (5nm, 10nm, 15nm) under 6000 Gs transverse magnetic field.

The ionization of air were tested by device coated with 5nm Mn out of magnetic field, in 6000Gs transverse magnetic field, and 6000Gs longitudinal magnetic field (Longitudinal magnetic field could reduce the lateral diffusion of electrons and effectively increase the collision frequency between electrons and the gas molecules, thus increasing the ionization efficiency) [87],

which results are shown in Fig.4.8. Without magnetic field, there is no ionization even though the applied voltage increases to 210 V, which means the breakdown voltage of air is higher than 210 V for 5 nm Mn decorated ZnO nano-rod device. Once applying magnetic field, the breakdown voltage drops lower than 30V, no matter magnetic field direction is parallel or perpendicular to device plane, which is good enough to be powered by portable batteries. There is no obvious difference between the two directions of magnetic field. It is clearly seen that the breakdown voltage of air is decreased more than 10 times with 5nm Mn decoration under 6000Gs magnetic field.

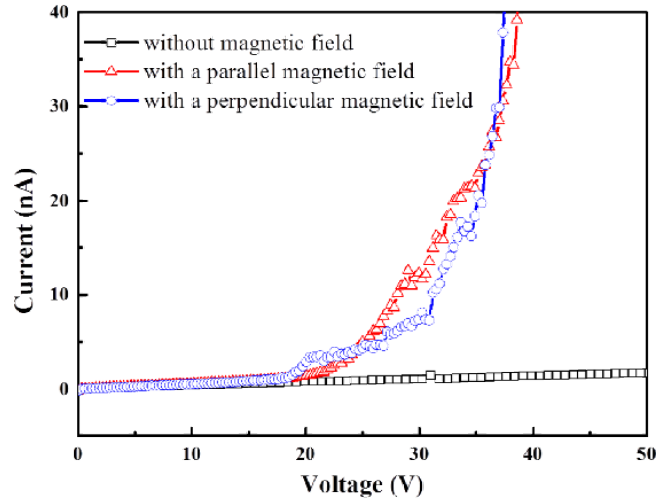


Figure 4.8 Air ionization for a 5 nm Mn decorated ZnO nano-rods electrode under 6000 Gs parallel and perpendicular magnetic field.

Actually, in a crossed magnetic and electric field, the breakdown voltage is expressed as:

$$V_{EB} = \frac{B_k^k p d \sqrt{1 + C(B^2 / P^2)}}{\left[ \ln A_k / \Gamma_k + \ln \left( p d \sqrt{1 + C(B^2 / P^2)} \right) \right]^k} \quad (5.1)$$

Where  $p$  is the gas pressure in unit of Torr,  $k$  has been empirically determined to be one for the molecular gases and two for the atomic gases.  $A_k$  and  $B_k$  is the coefficients, for nitrogen  $A_k$

$=12\text{cm}^{-1}\text{Torr}^{-1}$  and  $B_k=342\text{Vcm}^{-1}\text{Torr}^{-1}$ .  $B$  is the magnetic flux density expressed in Gauss and  $C$  is a constant.  $\Gamma_k$  is related to the value of yield per ion  $\gamma$  as  $\Gamma_k = \ln\left(1 + \frac{1}{\gamma}\right)$ . It was confirmed that  $V_{EB}$  can be effectively decreased by magnetic field. As seen from equation (1), the breakdown voltage has a minimum value against magnetic field.

In order to confirm if the gas ionization voltage is still the distinct character for different gases when the anode ZnO nano-rod arrays are decorated with metal and working under magnetic field, 6% IPA was introduced to the device coated by 5nm Mn under 6000Gs transverse magnetic field. Fig.4.9 shows the ionization results of 6% IPA and air by the same device. The breakdown voltages are well separated between 6% IPA and air. Moreover, the breakdown voltage for 6% IPA has been reduced from 17V to 5V comparing with pristine ZnO nano-rod array device, which result is shown in Fig.4.4.

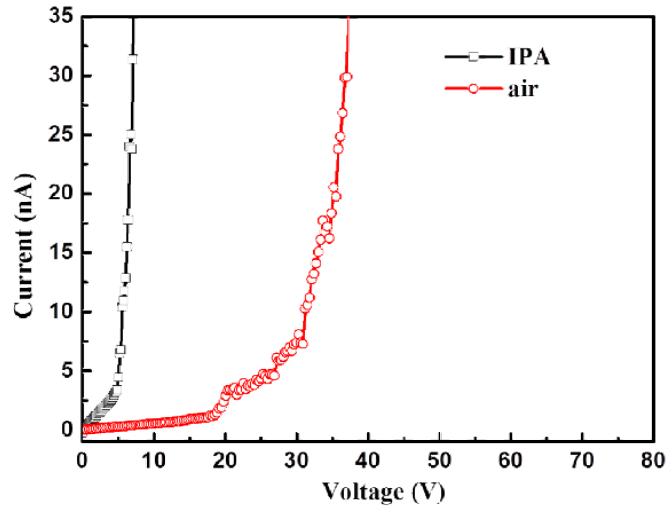


Figure 4.9 6% IPA and air ionization for a 5 nm Mn decorated ZnO nano-rods electrode under 6000 Gs transverse magnetic field.

### **4.3 Conclusion**

The low voltage air ionization sensor based on ZnO nano-rods electrode was explored. It was found that metal decoration and magnetic field can effectively reduce the electrical breakdown voltage of gases. The metal decoration increases the surface roughness and thus increases the electrical field emission, while magnetic field confines the motion of electron leading to increase the collision frequency between electrons and molecules, and thus increases the ionization efficiency.

## **Chapter 5 Self-powered active sensors based on 3D ZnO nanowire arrays**

As we know, the conventional metal oxide semiconductor gas sensor devices are connected to input power to initiate the sensing system. It is good enough for applications in industrial and normal life. However, if these sensors are used in some areas short of power, it has to find out the solution to power the devices. Generally, the devices could be powered by solar cells. However, it is still limited to the performance of the solar cells and has to be working in sunshine areas. Recently, researchers have intensively studied on a novel nanogenerators based on the piezoelectric, triboelectric or pyroelectric effect [88-90]. Nanogenerators based on nanotechnology have been able to convert trace energy in the environment into electric energy which could be collected as an efficient energy source for nanodevices and nanosystems. It is called a new self-powered system which is integrated from nanogenerator and functional nanodevice, aiming at harvesting tiny mechanical energy in the environment to power the nanodevice. The biggest advantage of this self-powered system is that it could be operated independently and wirelessly without energy storage or supply systems [91]. With the development of the self-powered systems, it could be widely used in medical science, environmental monitoring, defense technology as well as personal electronics due to their great adaptability and mobility.

### **5.1 Experiment**

To start the experiment,  $2 \times 2\text{cm}^2$  GaN/Al<sub>2</sub>O<sub>3</sub> (0001) substrates were prepared. These substrates were first cleaned by standard method (ultrasonically cleaned by acetone, isopropyl alcohol (IPA), and deionized water successively), and dried under a nitrogen flow, followed by growing vertical ZnO nanowire arrays in autoclave.

Hydrothermal synthesis was employed for vertical ZnO nanowires growth on  $2 \times 2\text{cm}^2$  GaN/Al<sub>2</sub>O<sub>3</sub> (0001) substrate. The one step growth was carried out in the nutrition solution of 50 mM/L mixture of Zn(NO<sub>3</sub>)<sub>2</sub> and hexamethylenetetramine (HMTA) with 1:1 mass ratio in deionzied water at 80°C for 5 hours.

Shell layers of 50 nm SnO<sub>2</sub>, In<sub>2</sub>O<sub>3</sub>, and WO<sub>3</sub> were sputtered in a Lesker PVD75 system with a deposition rate range of 0.2~0.5 Angstrom/s at room temperature. 100nm Au is sputtered on the corner on the substrate as bottom electrode by Cressington 308R system. 100nm Pt is sputtered on Kapton film as top electrode by Cressington 308R system. Fig.5.1 is the Schematics of fabrication 3D core/shell nanowire array self-powered active sensors. Core/shell nanowire arrays are sandwiched by kapton coated Pt and GaN substrate.

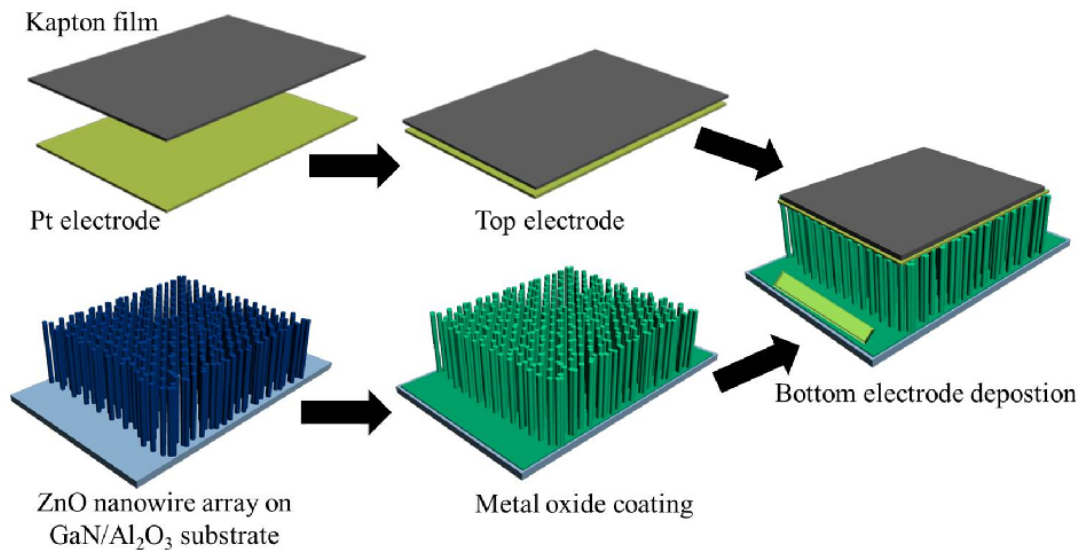


Figure 5.1 Schematics of fabrication 3D core/shell nanowire array self-powered active sensors.

Flexible Kapton film is able to enhance the effective contacts between the top electrode and nanowire arrays [92]. Even if NW arrays had moderate alignments and light height difference, flexible Kapton is soft enough to be bent to follow the height profiles of nanowire arrays. With compressive deformation on nanowire arrays, the piezoelectric output voltage of the device could

be observed by the connected voltmeter and the value changes depend on the targeting gases in the environment. All the experiments are handled in normal atmosphere at room temperature.

One thing needs to be mentioned is the thickness of the device is depending on the lengths of nanowires. Generally, nanowire lengths in this experiment are around  $7\mu\text{m}$ , which may obstruct the infiltration of the test gas. Wang et al. developed a piezoelectric oxygen sensor using an individual ZnO NW laterally-located on a flexible substrate, in which the test gas could be easier in contact with the NW. In the future work, the device structure should be further improved to facilitate the gas infiltration, such as to grow longer nanowires, to develop laterally-aligned nanoarrays on the flexible substrate, or to prepare porous top electrodes [89].

## 5.2 Result and discussion

Fig.5.2 shows the piezoelectric output voltage of  $\text{SnO}_2/\text{ZnO}$  nanowire arrays in dry air, 1000ppm  $\text{H}_2\text{S}$  and 1000ppm  $\text{NO}_2$  under the same applied strain at room temperature. Compared these three plots in Fig.5.2, we could see the output in 1000ppm  $\text{H}_2\text{S}$  is lower than output in air, but the output in 1000 ppm  $\text{NO}_2$  is higher than output in air. That is because of different properties of  $\text{H}_2\text{S}$  and  $\text{NO}_2$ , since  $\text{H}_2\text{S}$  is reducing gas, and  $\text{NO}_2$  is oxidizing gas.

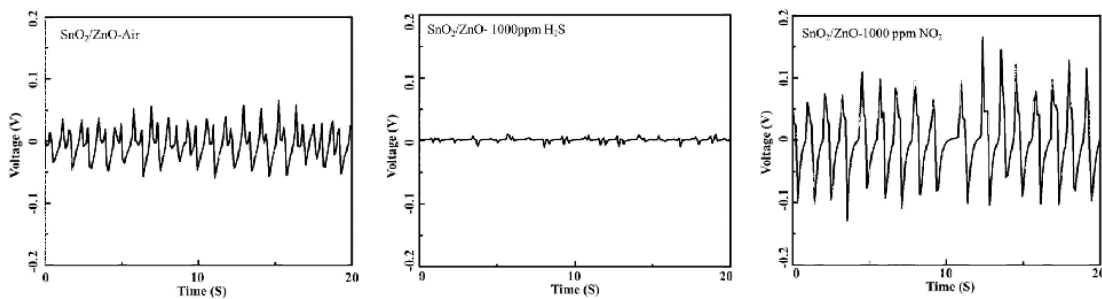


Figure 5.2 Piezoelectric output voltage of  $\text{SnO}_2/\text{ZnO}$  nanowire arrays in dry air, 1000ppm  $\text{H}_2\text{S}$  and 1000ppm  $\text{NO}_2$  under the same applied strain at room temperature.

The sensitivity and operation temperature are regarded as key parameters to evaluate the sensor performance. 3D  $\text{SnO}_2/\text{ZnO}$  nanogenerator as a self-powered active sensor works at room

temperature and it is good for its future application because of no need extra power consumption. This active sensor is able to detect both reducing gas and oxidizing gas, so it has potential to be used in different fields.

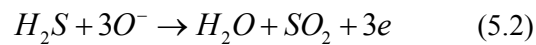
The sensitivity of self-powered active sensor could be defined as:

$$S\% = \frac{V_g - V_a}{V_a} \times 100\% \quad (5.1)$$

Where  $V_g$  is output in targeting gases, and  $V_a$  is output in air under same strain and same temperature.

Both ZnO and SnO<sub>2</sub> are known n-type semiconductors in nature. The work functions of ZnO and SnO<sub>2</sub> are 5.2 and 4.9 eV, and the band gaps are 3.37 and 3.5 eV, respectively [93]. The n-n hetero-junction will be formed on the interface between ZnO and SnO<sub>2</sub>, and the electrons flow from low work function SnO<sub>2</sub> into high work function ZnO until equilibrium on their Fermi levels. Their energy band bends at the surface and the built-in-potential at the interface between ZnO and SnO<sub>2</sub> equals their work function difference (0.3 eV) [94].

The detailed sensing mechanism of 3D SnO<sub>2</sub>/ZnO as a self-powered active sensor to detect H<sub>2</sub>S is shown in Fig.5.3. For self-powered active sensor, SnO<sub>2</sub>/ZnO nanowire arrays have two functions of an energy source and gas sensor. That is because the SnO<sub>2</sub>/ZnO nanowire arrays can produce piezoelectric output power under strain and piezoelectric outputs of SnO<sub>2</sub>/ZnO nanowire arrays varies under different atmospheres [31]. At room temperature, the physical adsorbed H<sub>2</sub>S molecules can react with these oxygen species. As described by



The reducing reacting will reverse the band bending and release the electrons back to conducting band, leading to an increased conductivity. Meanwhile, the generated H<sub>2</sub>O molecules can be adsorbed on nanowire surface, which can influence the depletion region the conductivity. Generally, H<sub>2</sub>O molecules can be adsorbed on the surface of nanostructures by physisorption or

hydrogen bonding. At high temperature, H<sub>2</sub>O molecules can react with the Lewis acid site (Sn) and Lewis base site (O) on the SnO<sub>2</sub> surface and then release electrons. At room temperature, H<sub>2</sub>O molecules can displace the pre-adsorbed oxygen on the surface of SnO<sub>2</sub> by competitive water physisorption, and increase the amount of free electrons [95]. Compared with the device in air, the device in H<sub>2</sub>S will more conductive and more electrons will be on the surface of SnO<sub>2</sub>/ZnO nanowires. Free electrons in the conduction band tend to flow and screen the positive ionic piezoelectric charges at one end, while leaving the negative ionic piezoelectric charges alone.

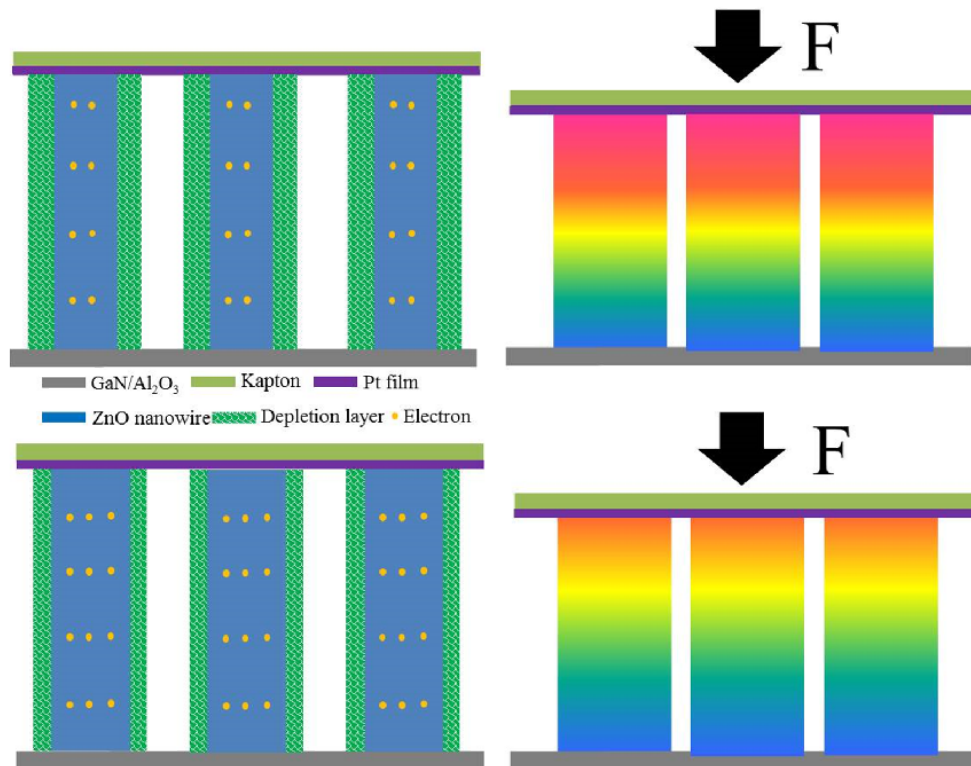
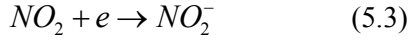


Figure 5.3 Working mechanism of self-powered active gas sensor based on 3D SnO<sub>2</sub>/ZnO nanowire arrays-top two are in air and bottom two are in H<sub>2</sub>S.

When the device in air is under compressive strain, a piezoelectric field is created along SnO<sub>2</sub>/ZnO nanowires. Free electrons in the conduction band tend to flow and screen the positive ionic piezoelectric charges at one end, while leaving the negative ionic piezoelectric charges alone [96]. When the compressive strain is added on the device in H<sub>2</sub>S, piezoelectric field will be

also created along SnO<sub>2</sub>/ZnO nanowires. More free electrons in SnO<sub>2</sub>/ZnO nanowires can flow and screen the piezoelectric field. The screening effect will lead lower piezoelectric output [97].

On contrary, oxidizing gases like NO<sub>2</sub> would decrease the device conductance. As described by



When exposed to NO<sub>2</sub>, the density of free electrons at the nanowire surface is reduced and the depletion layer is widened, resulting in an increased piezoelectric output.

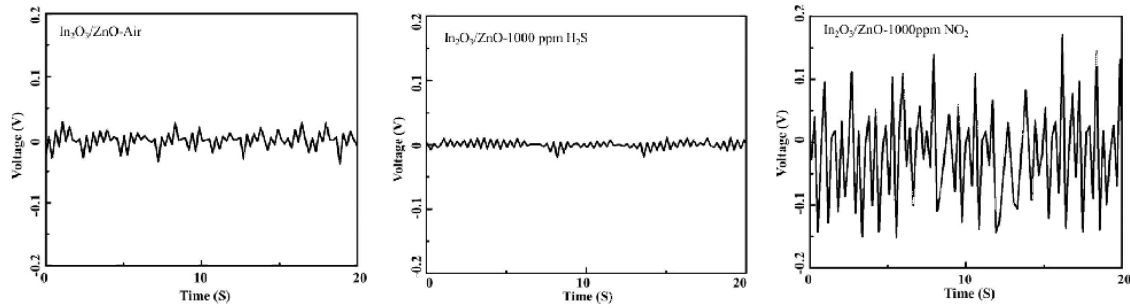


Figure 5.4 Piezoelectric output voltage of In<sub>2</sub>O<sub>3</sub>/ZnO nanowire arrays in dry air, 1000ppm H<sub>2</sub>S and 1000ppm NO<sub>2</sub> under the same applied strain at room temperature.

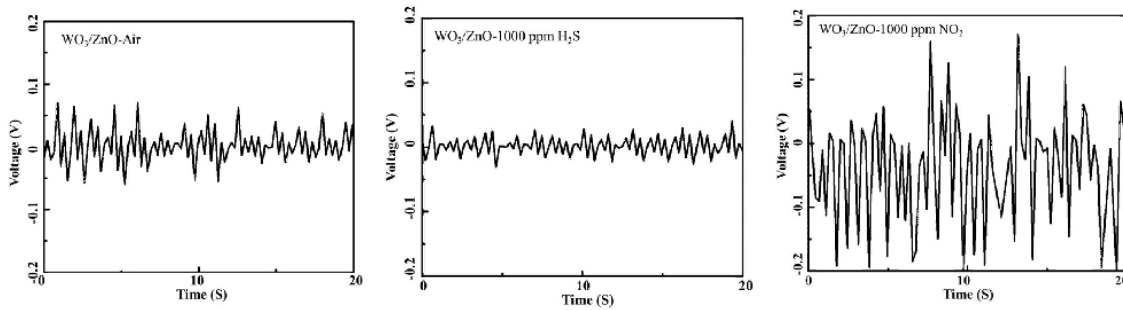


Figure 5.5 Piezoelectric output voltage of WO<sub>3</sub>/ZnO nanowire arrays in dry air, 1000ppm H<sub>2</sub>S and 1000ppm NO<sub>2</sub> under the same applied strain at room temperature.

Self-powered active sensor based on In<sub>2</sub>O<sub>3</sub>/ZnO and WO<sub>3</sub>/ZnO nanowire arrays are also fabricated. Fig.5.4 shows the testing of In<sub>2</sub>O<sub>3</sub>/ZnO nanowire arrays and Fig.5.5 exhibits the testing of WO<sub>3</sub>/ZnO nanowire arrays in dry air, 1000ppm H<sub>2</sub>S and 1000ppm NO<sub>2</sub> under the same applied strain at room temperature. We found both devices have responses to 1000ppm H<sub>2</sub>S and 1000ppm NO<sub>2</sub> and have the same trend with SnO<sub>2</sub>/ZnO nanowire array device, since both In<sub>2</sub>O<sub>3</sub>

and  $\text{WO}_3$  are n-type semiconductors. However, the responses varies compared these different devices even under the same strain in the same atmospheres, that may be due to the different work functions of the shell layer metal oxides.

### **5.3 Conclusions**

The nanogenerators have successfully fabricated by 3D  $\text{SnO}_2/\text{ZnO}$ ,  $\text{In}_2\text{O}_3/\text{ZnO}$  and  $\text{WO}_3/\text{ZnO}$  nanowire arrays. All the nanogenerators could be used to detect  $\text{H}_2\text{S}$  and  $\text{NO}_2$  without extra power consumption. The novel self-powered active sensor has big potential to be improved in the future by replacing the sensing materials with high performance and controlling the structures of the devices.

## Chapter 6 ZnO nanowire arrays SAW sensor

SAW sensors are sensitive to physical stimulus as well as chemical stimulus, such as additional mass, temperature, strain, and chemical reactions. To improve the performance of SAW sensors, it is a good way to increase the surface area of the sensing materials to enhance contact probability with targeting gases [98]. 3D ZnO nanowire arrays will be fabricated on SAW substrate assisted with e-beam lithography technique due to the extremely large surface. With e-beam lithography technique, the nanowire arrays could be designed to better serve SAW sensors.

### 6.1 Experiment

SAW devices are fabricated on piezoelectric ST-cut quartz substrates. The central frequency of SAW device is 198.8 MHz and insertion loss is -15.5 dB. Both input and output IDTs have 30 pairs of fingers, and the width of each finger is 4 $\mu$ m, and the aperture of the IDTs is 3 mm. When are connected to power on both side, the ST-cut quartz substrate would be excited and produced surface acoustic wave, spreading along the surface with the wavelength of 16 $\mu$ m, due to the piezoelectric effect of ST-cut quartz substrate.

ZnO/SiO<sub>2</sub>(Z/S) composite prepared by the sol-gel method was spin-coated onto the SAW devices at a speed of 6000 r/min for 30s. Then, the as-coated devices were immediately pre-heated for 10mins at 300 $^{\circ}$ C. After repeating these two steps three times, the SAW device was calcined for 2h at 480  $^{\circ}$ C in air to form the firm ZnO/SiO<sub>2</sub> composite film.

### 6.2 Results and discussion

The SEM images of pure ZnO film and Z/S composite films with Z/S ratio of 1:1 and 1:2 are shown in Fig.6.1. Pure ZnO film was flat and dense in Fig.6.1a, which consisted of uniform ZnO particles of average 15nm, while the surfaces become rough shown in Fig.6.1b and Fig.6.1c,

which may enhance the sensitivity of the gas sensor due to the larger surface area.

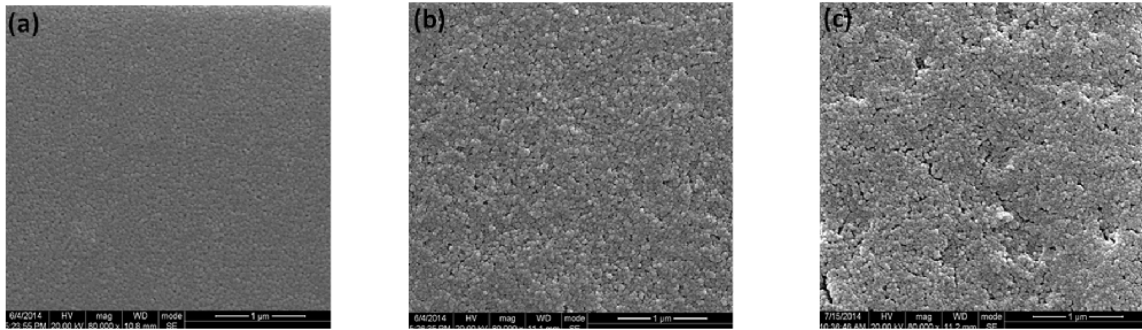


Figure 6.1 SEM image of (a) pure ZnO film, (b) Z/S film (R=1:1) and (c) ZS film (R=1:2)

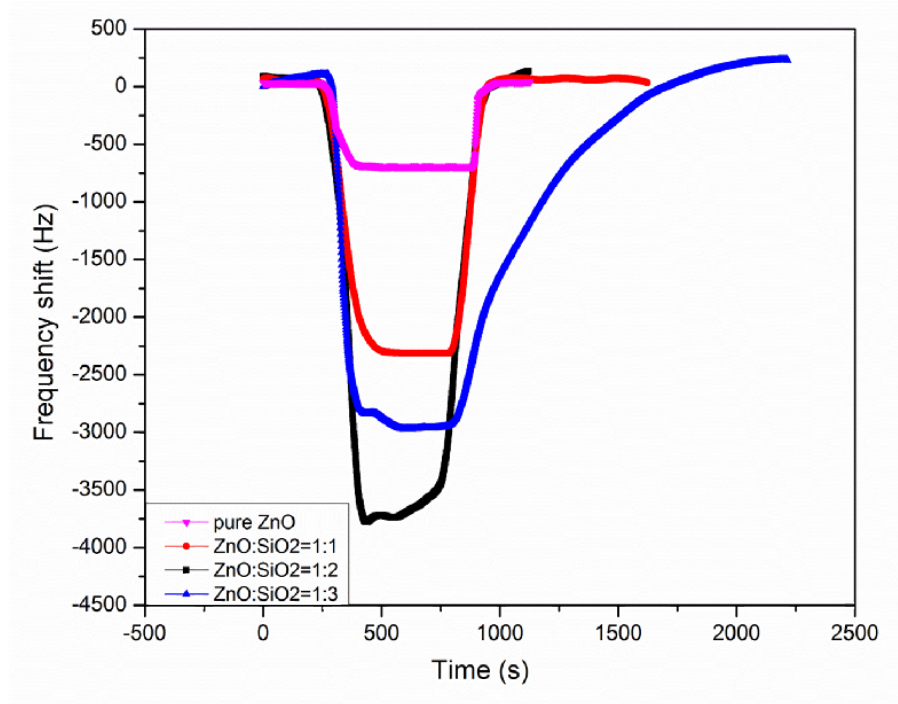


Figure 6.2 Sensing responses of saw devices to 50ppm ammonia at room temperature.

Fig.6.2 shows the sensing responses of saw devices coated different Z/S ratio films to 50ppm  $\text{NH}_3$  (diluted by air) at room temperature. All devices coated by Z/S composite films exhibited better sensing performance than the one coated by pure ZnO film. Moreover, the one coated by 1:2 Z/S film shows the best sensitivity with frequency shift of 3.84 kHz.

The devices coated by pure ZnO film and 1:2 Z/S composite film were put in the testing chamber to measure the sensing response to NH<sub>3</sub> gas with sequence concentration of 10ppm, 20ppm, 50ppm, 100ppm, and 200ppm at room temperature. The testing result is shown in Fig.6.3. The responses of the sensor based on a pure ZnO film were 98 Hz, 235 Hz, 720Hz, 1.52 kHz, and 2.86 kHz, while the the responses of the sensor based on 1:2 Z/S film were 1.132 kHz, 1.95 kHz, 3.84 kHz, 5.15 kHz, and 8.276 kHz respectively. Compared with the sensor based on pure ZnO film, the one coated by 1:2 Z/S film have much better sensitivity for same concentration NH<sub>3</sub>. Especially at low concentration 10ppm NH<sub>3</sub>, the response is one order magnitude larger than that the one coated by pure ZnO film.

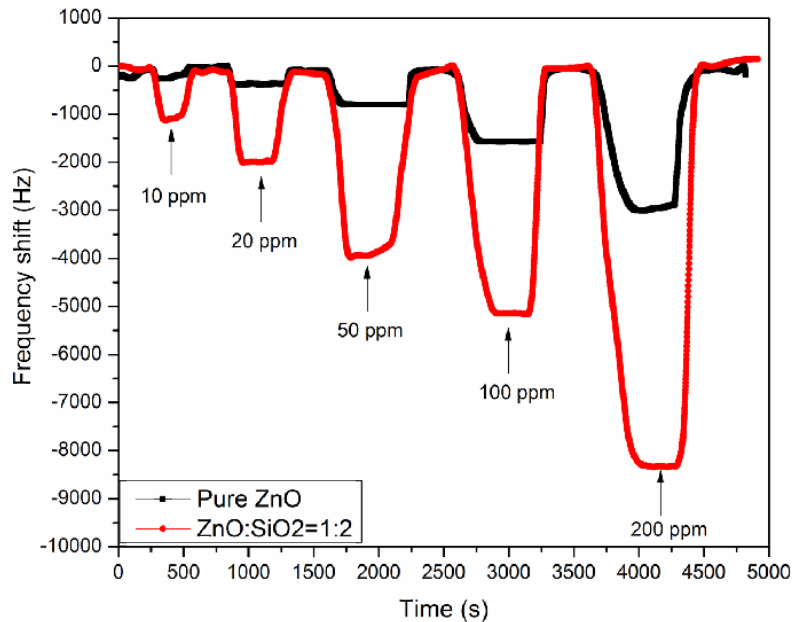


Figure 6.3 Sensing responses towards different concentrations of ammonia at room temperature.

The sensor based on 1:2 Z/S film were tested to reducing gases of C<sub>2</sub>H<sub>6</sub>O, CO, and H<sub>2</sub>, and oxidizing gas NO<sub>2</sub>, respectively and all concentrations of gases are 100ppm, as shown in Fig.6.4. Compared with the frequency shift of 5.27 kHz to targeting NH<sub>3</sub> gas, the responses to non-targeting gases are weak and negligible, suggesting the sensor has an excellent selectivity to NH<sub>3</sub>.

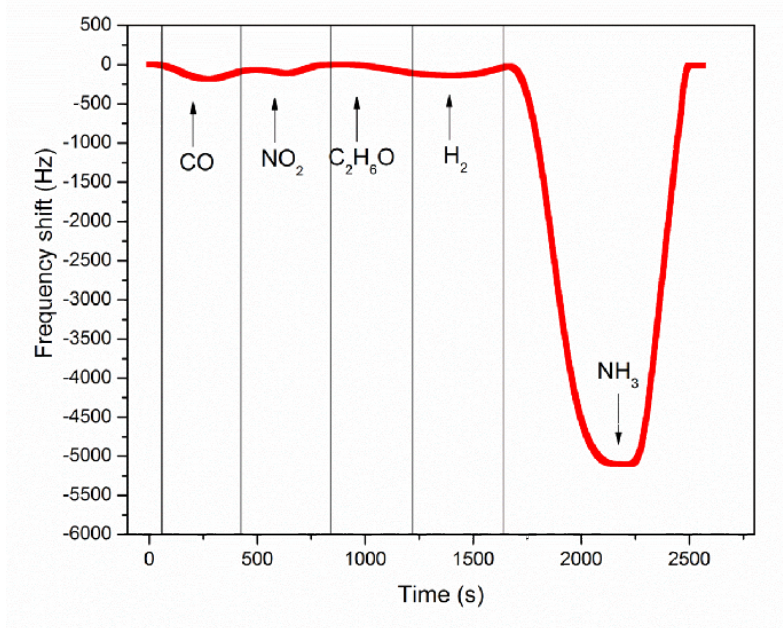


Figure 6.4 Sensing responses of device coated with 1:2 Z/S film to different gases under 100ppm.

### 6.3 Conclusion and future plan

SAW devices of 1:2 Z/S coated on piezoelectric ST-cut quartz substrate have shown good sensitivity on selectivity on NH<sub>3</sub> detection.

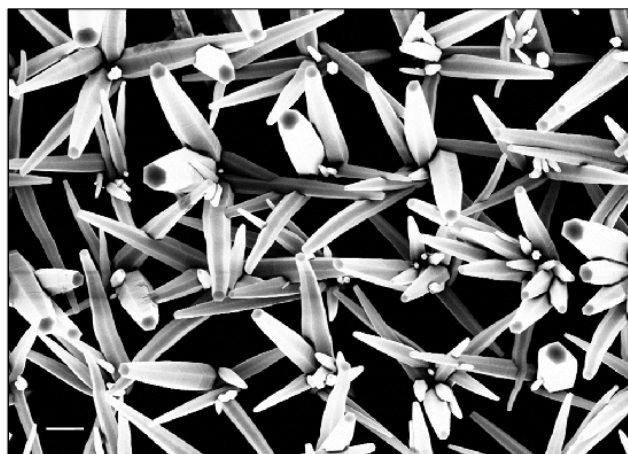


Figure 6.5 FESEM image of 3D ZnO nanowire array grown on piezoelectric ST-cut quartz substrates. (Scale bar 1 μm)

3D ZnO nanowire arrays are able to grow on piezoelectric ST-cut quartz substrates by hydrothermal method, as shown in Fig.6.5. Due to the large surface area of 3D ZnO nanowire arrays, the device performance are expected to be much better improved. Moreover, the e-beam lithography technique would be employed to precise control the growth the nanowire arrays under desired design, which may provide a way to tune the sensitivity and selectivity of the devices.

## Chapter 7 Conclusions

In this dissertation, we employed 3D ZnO nanowire arrays to build 3D gas sensors which operate on different physical principals including chemoresistance, piezoelectric effect, gas ionization, and surface acoustic waves. The goal is to develop a novel gas-sensing device based on these sensor technologies that can mimic a mammal's olfactory system, sometimes referred to as an "electronic nose". The complexity of the system requires several sensing techniques, since each technique has its own advantages and drawbacks in real applications. These advantages and drawbacks (mainly in sensitivity and selectivity) are functions of the sensing technique and the materials used as the sensing element. 3D nanowire arrays are used since they have extremely large surface areas, similar to receptors in mammal olfactory systems. Several devices have successfully been fabricated and have good sensitivity to targeting gases. The traditional semiconductor gas sensor, based on chemoresistance, fabricated using ZnO nanowire arrays decorated with SnO<sub>2</sub>, In<sub>2</sub>O<sub>3</sub> and WO<sub>3</sub> has shown good selectivity to several technologically and environmentally important gases including NO<sub>2</sub>, H<sub>2</sub>S, H<sub>2</sub>, NH<sub>3</sub> and CO. Self-powered active sensors were fabricated based on the piezoelectric effect. This can be considered a "green" sensor system, since it does not need extra power. Our self-powered active sensors have shown good detection for H<sub>2</sub>S and NO<sub>2</sub>, also could discriminate between these gasses by measuring the induced voltage change for a given pressure stimulus. PEDOT:PSS conducting polymer sensors have good capability for detection volatile organic gas, and the sensing properties can be adjusted by adding metal oxides. Ionization gas sensors are able to ionize air with safe operation voltages. Finally, we also fabricated and investigated the properties of surface acoustic wave (SAW) sensors using mixture of ZnO/SiO<sub>2</sub>. In the future, in addition to sensitivity and selectivity studied in this thesis, other properties of the 3D nanowire devices like stability and life cycle will need to be established in order to commercialize these devices.

## References

- [1] J. Janata, M. Josowicz, P. Vanýsek, and D. M. DeVaney, "Chemical sensors," *Analytical Chemistry*, vol. 70, pp. 179-208, 1998.
- [2] D. M. Wilson, S. Hoyt, J. Janata, K. Booksh, and L. Obando, "Chemical sensors for portable, handheld field instruments," *Sensors Journal, IEEE*, vol. 1, pp. 256-274, 2001.
- [3] U. Yogeswaran and S.-M. Chen, "A review on the electrochemical sensors and biosensors composed of nanowires as sensing material," *Sensors*, vol. 8, pp. 290-313, 2008.
- [4] J. R. Stetter, W. R. Penrose, and S. Yao, "Sensors, chemical sensors, electrochemical sensors, and ECS," *Journal of The Electrochemical Society*, vol. 150, pp. S11-S16, 2003.
- [5] K. J. Albert, N. S. Lewis, C. L. Schauer, G. A. Sotzing, S. E. Stitzel, T. P. Vaid, et al., "Cross-reactive chemical sensor arrays," *Chemical reviews*, vol. 100, pp. 2595-2626, 2000.
- [6] L. Ruiz-Garcia, L. Lunadei, P. Barreiro, and I. Robla, "A review of wireless sensor technologies and applications in agriculture and food industry: state of the art and current trends," *Sensors*, vol. 9, pp. 4728-4750, 2009.
- [7] Y. Wang and J. T. Yeow, "A review of carbon nanotubes-based gas sensors," *Journal of Sensors*, vol. 2009, 2009.
- [8] J. Chen, K. Wang, and W. Zhou, "Vertically Aligned ZnO Nanorod Arrays Coated with SnO<sub>2</sub>/Noble Metal Nanoparticles for Highly Sensitive and Selective Gas Detection," *Nanotechnology, IEEE Transactions on*, vol. 10, pp. 968-974, 2011.
- [9] B. Cao, J. Chen, X. Tang, and W. Zhou, "Growth of monoclinic WO<sub>3</sub> nanowire array for highly sensitive NO<sub>2</sub> detection," *Journal of Materials Chemistry*, vol. 19, pp. 2323-2327, 2009.

- [10] L. de Angelis and R. Riva, "Selectivity and stability of a tin dioxide sensor for methane," *Sensors and Actuators B: Chemical*, vol. 28, pp. 25-29, 1995.
- [11] Y. Cui, Q. Wei, H. Park, and C. M. Lieber, "Nanowire nanosensors for highly sensitive and selective detection of biological and chemical species," *Science*, vol. 293, pp. 1289-1292, 2001.
- [12] S. R. Morrison, "Semiconductor gas sensors," *Sensors and Actuators*, vol. 2, pp. 329-341, 1982.
- [13] C. Wilbertz, H.-P. Frerichs, and T. Kolleth, "Semiconductor gas sensor," ed: Google Patents, 2013.
- [14] J. O. Barnes and D. J. Leary, "Semiconductor gas sensor," ed: Google Patents, 1984.
- [15] S. R. Morrison, "Mechanism of semiconductor gas sensor operation," *Sensors and Actuators*, vol. 11, pp. 283-287, 1987.
- [16] N. Yamazoe, Y. Kurokawa, and T. Seiyama, "Effects of additives on semiconductor gas sensors," *Sensors and Actuators*, vol. 4, pp. 283-289, 1983.
- [17] P. Moseley and B. Tofield, "Semiconductor gas sensors," *Materials science and technology*, vol. 1, pp. 505-509, 1985.
- [18] J. J. Miasik, A. Hooper, and B. C. Tofield, "Conducting polymer gas sensors," *Journal of the Chemical Society, Faraday Transactions 1: Physical Chemistry in Condensed Phases*, vol. 82, pp. 1117-1126, 1986.
- [19] P. N. Bartlett and S. K. Ling-Chung, "Conducting polymer gas sensors Part III: Results for four different polymers and five different vapours," *Sensors and Actuators*, vol. 20, pp. 287-292, 1989.
- [20] P. N. Bartlett, P. Archer, and S. K. Ling-Chung, "Conducting polymer gas sensors part I: fabrication and characterization," *Sensors and Actuators*, vol. 19, pp. 125-140, 1989.
- [21] J. M. Slater, J. Paynter, and E. Watt, "Multi-layer conducting polymer gas sensor arrays for olfactory sensing," *Analyst*, vol. 118, pp. 379-384, 1993.

- [22] J. W. Gardner and P. Bartlett, "Design of conducting polymer gas sensors: modelling and experiment," *Synthetic Metals*, vol. 57, pp. 3665-3670, 1993.
- [23] J. Janata and M. Josowicz, "Conducting polymers in electronic chemical sensors," *Nature materials*, vol. 2, pp. 19-24, 2003.
- [24] T. T. Ma, "Ionization sensor," ed: Google Patents, 1991.
- [25] A. Saitzkoff, R. Reinmann, F. Mauss, and M. Glavmo, "In-cylinder pressure measurements using the spark plug as an ionization sensor," *SAE Technical Paper*1997.
- [26] A. Franke, R. Reinmann, and A. Larsson, "The role of the electrodes for the ionization sensor signal," *SAE Technical Paper*2003.
- [27] U. Bonne, "Gas ionization sensor," ed: Google Patents, 2003.
- [28] R. B. Sadeghian and M. Kahrizi, "A novel miniature gas ionization sensor based on freestanding gold nanowires," *Sensors and Actuators A: Physical*, vol. 137, pp. 248-255, 2007.
- [29] L. Liao, H. Lu, M. Shuai, J. Li, Y. Liu, C. Liu, et al., "A novel gas sensor based on field ionization from ZnO nanowires: moderate working voltage and high stability," *Nanotechnology*, vol. 19, p. 175501, 2008.
- [30] Z. L. Wang, "Towards Self-Powered Nanosystems: From Nanogenerators to Nanopiezotronics," *Advanced Functional Materials*, vol. 18, pp. 3553-3567, 2008.
- [31] Z. L. Wang, "Self-Powered Nanosensors and Nanosystems," *Advanced Materials*, vol. 24, pp. 280-285, 2012.
- [32] M. Nieuwenhuizen and A. Nederlof, "A SAW gas sensor for carbon dioxide and water. Preliminary experiments," *Sensors and Actuators B: Chemical*, vol. 2, pp. 97-101, 1990.
- [33] L. J. Kepley, R. M. Crooks, and A. J. Ricco, "A selective SAW-based organophosphonate chemical sensor employing a self-assembled, composite monolayer: a new paradigm for sensor design," *Analytical Chemistry*, vol. 64, pp. 3191-3193, 1992.

- [34] M. Von Schickfus, R. Stanzel, T. Kammereck, D. Weiskat, W. Dittrich, and H. Fuchs, "Improving the SAW gas sensor: device, electronics and sensor layer," *Sensors and Actuators B: Chemical*, vol. 19, pp. 443-447, 1994.
- [35] Y. Lee, H. Kim, Y. Roh, H. Cho, and S. Baik, "Development of a saw gas sensor for monitoring SO<sub>2</sub> gas," *Sensors and Actuators A: Physical*, vol. 64, pp. 173-178, 1998.
- [36] S. Qin, Z. Wu, Z. Tang, Y. Song, F. Zeng, and D. Zhao, "The sensitivity to SO<sub>2</sub> of the SAW gas sensor with triethanolamine modified with boric acid," *Sensors and Actuators B: Chemical*, vol. 66, pp. 240-242, 2000.
- [37] M. Penza, P. Aversa, G. Cassano, W. Wlodarski, and K. Kalantar-Zadeh, "Layered SAW gas sensor with single-walled carbon nanotube-based nanocomposite coating," *Sensors and actuators B: Chemical*, vol. 127, pp. 168-178, 2007.
- [38] A. Sadek, W. Wlodarski, Y. Li, W. Yu, X. Li, X. Yu, et al., "A ZnO nanorod based layered ZnO/64° YX LiNbO<sub>3</sub> SAW hydrogen gas sensor," *Thin Solid Films*, vol. 515, pp. 8705-8708, 2007.
- [39] J. W. Gardner and P. N. Bartlett, *Sensors and sensory systems for an electronic nose*: Springer, 1992.
- [40] M. S. Freund and N. S. Lewis, "A chemically diverse conducting polymer-based" electronic nose", *Proceedings of the National Academy of Sciences*, vol. 92, pp. 2652-2656, 1995.
- [41] F. Röck, N. Barsan, and U. Weimar, "Electronic nose: current status and future trends," *Chemical reviews*, vol. 108, pp. 705-725, 2008.
- [42] T. C. Pearce, S. S. Schiffman, H. T. Nagle, and J. W. Gardner, *Handbook of machine olfaction: electronic nose technology*: John Wiley & Sons, 2006.
- [43] J. W. Gardner and P. N. Bartlett, *Electronic noses: principles and applications* vol. 233: Oxford University Press New York, 1999.

- [44] N. Barsan and U. Weimar, "Conduction model of metal oxide gas sensors," *Journal of Electroceramics*, vol. 7, pp. 143-167, 2001.
- [45] N. Barsan, D. Koziej, and U. Weimar, "Metal oxide-based gas sensor research: How to?," *Sensors and Actuators B: Chemical*, vol. 121, pp. 18-35, 2007.
- [46] R. Mönkemöller, "Metal-oxide gas sensor," ed: Google Patents, 2008.
- [47] C. Wang, L. Yin, L. Zhang, D. Xiang, and R. Gao, "Metal oxide gas sensors: sensitivity and influencing factors," *Sensors*, vol. 10, pp. 2088-2106, 2010.
- [48] E. Comini, "Metal oxide nano-crystals for gas sensing," *Analytica chimica acta*, vol. 568, pp. 28-40, 2006.
- [49] H. Lorenz, M. Stöger-Pollach, S. Schwarz, K. Pfaller, B. Klötzer, J. Bernardi, et al., "A new preparation pathway to well-defined In<sub>2</sub>O<sub>3</sub> nanoparticles at low substrate temperatures," *The Journal of Physical Chemistry C*, vol. 112, pp. 918-925, 2008.
- [50] C. Li, D. Zhang, X. Liu, S. Han, T. Tang, J. Han, et al., "In<sub>2</sub>O<sub>3</sub> nanowires as chemical sensors," *Applied Physics Letters*, vol. 82, pp. 1613-1615, 2003.
- [51] Z. W. Pan, Z. R. Dai, and Z. L. Wang, "Nanobelts of semiconducting oxides," *Science*, vol. 291, pp. 1947-1949, 2001.
- [52] H. J. Fan, R. Scholz, F. M. Kolb, and M. Zacharias, "Two-dimensional dendritic ZnO nanowires from oxidation of Zn microcrystals," *Applied physics letters*, vol. 85, pp. 4142-4144, 2004.
- [53] K. Yao, D. Caruntu, Z. Zeng, J. Chen, C. J. O'Connor, and W. Zhou, "Parts per billion-level H<sub>2</sub>S detection at room temperature based on self-assembled In<sub>2</sub>O<sub>3</sub> nanoparticles," *The Journal of Physical Chemistry C*, vol. 113, pp. 14812-14817, 2009.
- [54] W. Westwood, "Physical vapor deposition," in *Microelectronic Materials and Processes*, ed: Springer, 1989, pp. 133-201.
- [55] T. Takahashi, "Physical Vapor Deposition," in *Ultraclean Surface Processing of Silicon Wafers*, ed: Springer, 1998, pp. 352-360.

- [56] D. M. Mattox, Handbook of physical vapor deposition (PVD) processing: William Andrew, 2010.
- [57] S. M. Rossmagel, "Physical vapor deposition," Handbook of Semiconductor Manufacturing Technology, p. 395, 2000.
- [58] J. E. Mahan, "Physical vapor deposition of thin films," Physical Vapor Deposition of Thin Films, by John E. Mahan, pp. 336. ISBN 0-471-33001-9. Wiley-VCH, January 2000., vol. 1, 2000.
- [59] J.-H. Park and T. Sudarshan, Chemical vapor deposition vol. 2: ASM international, 2001.
- [60] S. Y. Bae, H. W. Seo, and J. Park, "Vertically aligned sulfur-doped ZnO nanowires synthesized via chemical vapor deposition," The Journal of Physical Chemistry B, vol. 108, pp. 5206-5210, 2004.
- [61] X. Liu, X. Wu, H. Cao, and R. Chang, "Growth mechanism and properties of ZnO nanorods synthesized by plasma-enhanced chemical vapor deposition," Journal of Applied Physics, vol. 95, pp. 3141-3147, 2004.
- [62] C.-L. Zhang, W.-N. Zhou, Y. Hang, Z. Lü, H.-D. Hou, Y.-B. Zuo, et al., "Hydrothermal growth and characterization of ZnO crystals," Journal of Crystal Growth, vol. 310, pp. 1819-1822, 2008.
- [63] S. Xu and Z. L. Wang, "One-dimensional ZnO nanostructures: solution growth and functional properties," Nano Research, vol. 4, pp. 1013-1098, 2011.
- [64] M. Kamalasanan and S. Chandra, "Sol-gel synthesis of ZnO thin films," Thin Solid Films, vol. 288, pp. 112-115, 1996.
- [65] C. Anderson and A. J. Bard, "An improved photocatalyst of TiO<sub>2</sub>/SiO<sub>2</sub> prepared by a sol-gel synthesis," The Journal of Physical Chemistry, vol. 99, pp. 9882-9885, 1995.
- [66] M. Paunovic, Electrochemical deposition: Wiley Online Library, 2006.
- [67] D. Grier, E. Ben-Jacob, R. Clarke, and L. Sander, "Morphology and microstructure in electrochemical deposition of zinc," Physical review letters, vol. 56, p. 1264, 1986.

- [68] J. Wang, X. Sun, Y. Yang, H. Huang, Y. Lee, O. Tan, et al., "Hydrothermally grown oriented ZnO nanorod arrays for gas sensing applications," *Nanotechnology*, vol. 17, p. 4995, 2006.
- [69] K. Wang, J. Chen, W. Zhou, Y. Zhang, Y. Yan, J. Pern, et al., "Direct growth of highly mismatched type II ZnO/ZnSe core/shell nanowire arrays on transparent conducting oxide substrates for solar cell applications," *Advanced Materials*, vol. 20, pp. 3248-3253, 2008.
- [70] J.-B. Lee, M.-H. Lee, C.-K. Park, and J.-S. Park, "Effects of lattice mismatches in ZnO/substrate structures on the orientations of ZnO films and characteristics of SAW devices," *Thin Solid Films*, vol. 447, pp. 296-301, 2004.
- [71] X. Liu, J. Zhang, L. Wang, T. Yang, X. Guo, S. Wu, et al., "3D hierarchically porous ZnO structures and their functionalization by Au nanoparticles for gas sensors," *Journal of Materials Chemistry*, vol. 21, pp. 349-356, 2011.
- [72] K. J. Choi and H. W. Jang, "One-dimensional oxide nanostructures as gas-sensing materials: review and issues," *Sensors*, vol. 10, pp. 4083-4099, 2010.
- [73] J. W. Gardner, "Detection of vapours and odours from a multisensor array using pattern recognition Part 1. Principal component and cluster analysis," *Sensors and Actuators B: Chemical*, vol. 4, pp. 109-115, 1991.
- [74] R. Dunia, S. J. Qin, T. F. Edgar, and T. J. McAvoy, "Identification of faulty sensors using principal component analysis," *AIChE Journal*, vol. 42, pp. 2797-2812, 1996.
- [75] A. M. Nardes, M. Kemerink, M. De Kok, E. Vinken, K. Maturová, and R. Janssen, "Conductivity, work function, and environmental stability of PEDOT: PSS thin films treated with sorbitol," *Organic Electronics*, vol. 9, pp. 727-734, 2008.
- [76] M. Kuş and S. Okur, "Electrical characterization of PEDOT: PSS beyond humidity saturation," *Sensors and Actuators B: Chemical*, vol. 143, pp. 177-181, 2009.

- [77] M. Berggren, R. Forchheimer, J. Bobacka, P.-O. Svensson, D. Nilsson, O. Larsson, et al., "PEDOT: PSS-based electrochemical transistors for ion-to-electron transduction and sensor signal amplification," in *Organic Semiconductors in Sensor Applications*, ed: Springer, 2008, pp. 263-280.
- [78] P. Lin and F. Yan, "Organic Thin-Film Transistors for Chemical and Biological Sensing," *Advanced materials*, vol. 24, pp. 34-51, 2012.
- [79] G. Harsányi, "Polymer films in sensor applications: a review of present uses and future possibilities," *Sensor Review*, vol. 20, pp. 98-105, 2000.
- [80] H. Yoon and J. Jang, "Conducting-polymer nanomaterials for high-performance sensor applications: issues and challenges," *Advanced Functional Materials*, vol. 19, pp. 1567-1576, 2009.
- [81] A. Guadarrama, J. Fernandez, M. Iniguez, J. Souto, and J. De Saja, "Array of conducting polymer sensors for the characterisation of wines," *Analytica chimica acta*, vol. 411, pp. 193-200, 2000.
- [82] R. B. Sadeghian and M. S. Islam, "Ultralow-voltage field-ionization discharge on whiskered silicon nanowires for gas-sensing applications," *Nature materials*, vol. 10, pp. 135-140, 2011.
- [83] A. Nikfarjam, F. Razi, and S. Z. Mortazavi, "Fabrication of gas ionization sensor using carbon nanotube arrays grown on porous silicon substrate," *Sensors and Actuators A: Physical*, vol. 162, pp. 24-28, 2010.
- [84] H. Wang, C. Zou, C. Tian, L. Zhou, Z. Wang, and D. Fu, "A novel gas ionization sensor using Pd nanoparticle-capped ZnO," *Nanoscale research letters*, vol. 6, pp. 1-4, 2011.
- [85] R. B. Sadeghian and M. Kahrizi, "A low voltage gas ionization sensor based on sparse gold nanorods," in *Sensors, 2007 IEEE*, 2007, pp. 648-651.

- [86] Z. Fan, D. Wang, P.-C. Chang, W.-Y. Tseng, and J. G. Lu, "ZnO nanowire field-effect transistor and oxygen sensing property," *Applied Physics Letters*, vol. 85, pp. 5923-5925, 2004.
- [87] J. Fraden, *Handbook of modern sensors: physics, designs, and applications*: Springer, 2004.
- [88] J. C. Engel, C. J. Luebke, J. J. Matsko, R. P. Shvach, and M. G. Solveson, "Self-powered power bus sensor employing wireless communication," ed: Google Patents, 2007.
- [89] Z. L. Wang, "Toward self-powered sensor networks," *Nano Today*, vol. 5, pp. 512-514, 2010.
- [90] S. Xu, Y. Qin, C. Xu, Y. Wei, R. Yang, and Z. L. Wang, "Self-powered nanowire devices," *Nature nanotechnology*, vol. 5, pp. 366-373, 2010.
- [91] S. Chakrabartty, N. G. Elvin, A. S. Gore, and N. Lajnef, "Self-powered sensor," ed: Google Patents, 2011.
- [92] P. Glynne-Jones and N. White, "Self-powered systems: a review of energy sources," *Sensor review*, vol. 21, pp. 91-98, 2001.
- [93] Y. Liu, E. Koep, and M. Liu, "A highly sensitive and fast-responding SnO<sub>2</sub> sensor fabricated by combustion chemical vapor deposition," *Chemistry of materials*, vol. 17, pp. 3997-4000, 2005.
- [94] K.-W. Kim, P.-S. Cho, S.-J. Kim, J.-H. Lee, C.-Y. Kang, J.-S. Kim, et al., "The selective detection of C<sub>2</sub>H<sub>5</sub>OH using SnO<sub>2</sub>-ZnO thin film gas sensors prepared by combinatorial solution deposition," *Sensors & Actuators: B. Chemical*, vol. 123, pp. 318-324, 2007.
- [95] B. T. Marquis and J. F. Vetelino, "A semiconducting metal oxide sensor array for the detection of NO<sub>2</sub> and NH<sub>3</sub>," *Sensors and Actuators B: Chemical*, vol. 77, pp. 100-110, 2001.
- [96] Z. L. Wang and J. Song, "Piezoelectric nanogenerators based on zinc oxide nanowire arrays," *Science*, vol. 312, pp. 242-246, 2006.

- [97] G. Zhu, R. Yang, S. Wang, and Z. L. Wang, "Flexible high-output nanogenerator based on lateral ZnO nanowire array," *Nano letters*, vol. 10, pp. 3151-3155, 2010.
- [98] R. Falconer, R. Lec, J. Vetelino, and Z. Xu, "Optimization of a SAW metal oxide semiconductor gas sensor," in *Ultrasonics Symposium, 1989. Proceedings., IEEE 1989, 1989*, pp. 585-590.

## **Vita**

Haiqiao Su was born in Nanyang, Henan province, China where he got his primary and high school educations. He obtained his bachelor and master degree in Physics department in University of Electronic Science and Technology of China (UESTC), Chengdu, Sichuan Province. He joined the Ph. D program of Engineering and Applied Sciences Program in Advanced Materials Research Institute, University of New Orleans. During his Ph. D program, he mainly focused on applications of gas sensors based on nanomaterials.